

# FINAL PUBLISHABLE REPORT

Grant Agreement number            14IND12  
 Project short name                    Innanopart  
 Project full title                        Metrology for innovative nanoparticles

Project start date and duration:		01 May 2015 (36 months)
Coordinator: Alex Shard, NPL Management Limited, Tel: +44 (0) 20 8977 3222 E-mail: <a href="mailto:Alex.Shard@npl.co.uk">Alex.Shard@npl.co.uk</a>		
Project website address: <a href="http://empir.npl.co.uk/innanopart/">http://empir.npl.co.uk/innanopart/</a>		
Internal Funded Partners:	External Funded Partners:	Unfunded Partners:
Partner 1 NPL, United Kingdom	Partner 7 BHAM, United Kingdom	Partner 12 INRIM, Italy
Partner 2 BAM, Germany	Partner 8 CEA, France	Partner 13 METAS, Switzerland
Partner 3 DFM, Denmark	Partner 9 WR, Netherlands	
Partner 4 LGC, United Kingdom	Partner 10 UPO, Italy	
Partner 5 PTB, Germany	Partner 11 TU WIEN, Austria	
Partner 6 SP, Sweden		

## Glossary

AES: Auger Electron Spectroscopy

BIPM-CCQM: Bureau International des Poids and Mesures - Consultative Committee for Amount of Substance: Metrology in Chemistry and Biology

CEN: European Committee for Standardisation

CPC: Condensation Particle Counter

DCS: Differential Centrifugal Sedimentation

DLS: Dynamic Light Scattering (also known as photon correlation spectroscopy, PCS)

DMA: Differential Mobility Analyser

ES-DMA-CPC: Electro Spray - Differential Mobility Analyser – Condensation Particle Counter

GIXRF: Grazing Incidence X-ray Fluorescence

HC-PCF: Hollow Core – Photonic Crystal Fibre

IC model: Infinitesimal Column model

ICPMS: Inductively Coupled Plasma Mass Spectrometry

ISO: International Organisation for Standardisation

ISS: Ion Scattering Spectroscopy

LEIS: Low Energy Ion Scattering

NAP-XPS: Near-ambient pressure X-ray photoelectron spectroscopy

PTA: Particle Tracking Analysis

SAM: Scanning Auger Microscopy

SAXS: Small Angle X-ray Scattering

SEM: Scanning Electron Microscopy

SESSA: Simulation of Electron Spectra for Surface Analysis

SHG: Second Harmonic Generation

SLA: Straight Line Approximation

STXM: Scanning Transmission X-ray Microscopy

spICPMS: single particle Inductively Coupled Plasma Mass Spectrometry

TEM: Transmission Electron Microscopy

TGA: Thermo-Gravimetric Analysis

TRPS: Tunable Resistive Pulse Sensing

UV-vis: Ultra Violet – visible photometry

VAMAS - TWA: Versailles Project on Advanced Materials and Standards – Technical Working Area

XPS: X-ray Photoelectron Spectroscopy

XSW: X-ray Standing Waves Spectrometry

XRS: X-ray Spectrometry



**TABLE OF CONTENTS**

1	Overview .....	4
2	Need.....	4
3	Objectives .....	4
4	Results .....	5
	Traceable Measurement of Particle Number Concentration .....	5
	Traceable Measurement of Shell Composition and Thickness .....	19
	Inter-laboratory studies .....	30
5	Impact .....	31
6	List of Publications .....	33
7	Contact details .....	33

## 1 Overview

Nanoparticles are increasingly used in innovative products manufactured by advanced industries and provide enhanced, unique properties of great commercial and societal value. The demand for high performance materials places increasingly stringent tolerances on the properties of nanoparticles. The major unmet metrological needs in the production of high quality nanomaterials are the measurement of particles' concentration surface chemistry. These measurements are critical to the performance of novel materials in products. To underpin trade and the supply chain for these novel materials, this project focused on the development of reference materials, compared the performance of different techniques, initiated pre-normalisation studies and provided input to internationally accepted standards.

## 2 Need

Europe has a significant share of both the ~€3bn global production and use of high performance nanoparticles and nanoparticle-enabled products, which is dominated by polymeric, noble metal and quantum dot nanomaterials. It is therefore essential to establish key measurement methods to support the manufacture, performance and reliability of such materials. Many types of innovative nanoparticles exist: metals used in catalysis, medical applications and conductive inks; metal oxides employed in fuel cells and ferrofluids, and as contrast agents for magnetic resonance imaging; semiconductors used as quantum dots and rods for bioimaging, photonics, display and lighting technologies; and organic particles used for electronic applications, drug delivery vehicles, fluorescent reporters and advanced coatings.

Measuring the concentration of nanoparticles in suspension is required to optimise and reproduce formulations and products. In most cases, this number concentration is not known but is calculated upon the basis of assumptions and mass-balance considerations. Currently, there are a number of methods which may be capable of measuring nanoparticle number concentration in colloidal suspension, but no standards or primary methods exist and no certified reference materials are available. The linearity, sample dependence, uncertainty and comparability of methods for the measurement of particle number concentration have not been established, even for ideal materials, and no validated reference materials exist for the calibration of commonly used instruments.

The surface chemistry of particles determines their behaviour and performance. Any surface modification, whether intentional or not, needs to be measured to fully understand the particles and their behaviour. Hence, measuring the surface chemistry of particles and quantifying the number of functional groups available for further reaction is fundamental to the successful formulation of products and their reliable operation. The amount of material in the surface layer, or 'shell', of the particle is determined by the chemistry of the shell and its thickness. This shell is often deliberately engineered to provide properties such as ease of dispersion, controlled agglomeration, biochemical recognition and the prevention of unwanted reactions such as protein adsorption, photocatalysis and quenching of optoelectronic properties. Robust measurement methods and standards are required for such measurements where they form a critical aspect of the design of the material.

Since these measurements are performed by researchers, manufacturers, contract analytical laboratories and customers it is essential that comparability between sites and instruments is established. Therefore there is a pressing need for good practice guides and standard procedures, preferably at an international level because of the global nature of trade in nanoparticles.

## 3 Objectives

The specific technical objectives of the project were to:

1. Develop traceable measurement and calibration protocols to measure particle number concentrations in liquid suspension with a target relative uncertainty of better than 10 %, improving the currently estimated 50 % uncertainty, for spherical particles in the size range 1 nm to 1000 nm.
2. Develop methods to quantify the number concentration of particles in partially agglomerated or aggregated states within a liquid suspension of otherwise monodisperse primary particles and the ability to measure number concentration of particles with a non-spherical shape.
3. Develop standard procedures to traceably measure the chemical composition and thickness of the nanoparticle shell, both to within 10 % uncertainty.

4. Conduct two inter-laboratory studies to establish a good practice guide for industry and thereby establish laboratory-scale methods to enable valid, routine monitoring and quality control of particle concentration and surface chemistry for nanoparticle-based formulations and products.
5. Engage with industry that manufactures and or / exploits nanoparticles in order to facilitate the uptake of the technology and measurement infrastructure developed by the project, to support the development of new, innovative products, thereby enhancing the competitiveness of EU industry.

The project additionally included an investigation of the effect of particle shape upon number concentration measurements for nanoparticles in a liquid suspension. The importance of non-spherical particles in innovative applications is growing and this additional activity addressed this emerging need.

## 4 Results

### Traceable Measurement of Particle Number Concentration

*This Chapter addresses Objectives 1 and 2*

#### 4.1.1 Introduction

The aim of this objective was to develop traceable methods for measuring particle number concentration for monodisperse, spherical reference materials with a target relative uncertainty of better than 10 %. By producing such particles and measuring their accurate concentrations, it is then feasible to provide reference materials with known number concentration which can be used to calibrate industrially relevant techniques.

Until this project, reference nanomaterials certified for particle number concentration were not available and it was not possible to produce them because confirmatory accurate measurements were not available. The state-of-the-art was to measure the total, dried mass of particles dispersed in liquid and, through estimations of particle volume and density, transform this into the particle number concentration. The inherent uncertainties and assumptions in the calculation meant that a factor of two uncertainty in the number concentration was considered reasonable. By direct measurements, using laboratory methods, stakeholders reported that uncertainties were so large that even obtaining the correct order of magnitude for particle concentration was considered a good result. The use of single particle counting methods which could measure colloidal particles removed the reliance upon particle density and volume information. However, this does not necessarily improve the certainty of the final measurements because there were open questions about the volume of liquid being sampled and the efficiency of detection, particularly as a function of particle size.

The measurement methods considered in this project are summarised in **Table 4.1.1**. The table provides an overview of whether the technique can measure number concentration using only simple extensions to the technique, it lists the measured quantities and, in the comments column, the sample constraints and information required to make a concentration measurement. Many of the techniques are also restricted in their ability to detect certain types, or sizes, of particles. Of the three techniques capable of direct and traceable measurements SAXS and spICPMS were selected to be developed in the project because the manner in which these could be made accurate was clear.

**Table 1:** Techniques capable of measuring colloidal particle number concentration used in this project.

Technique	Direct	Measured quantities	Comments
SAXS	Y	Angular dependent scattered X-ray intensity	Restricted to monodisperse spherical particles Requires electron density and optical path length
spICPMS	Y	Number of events	Restricted to dilute particles with detectable species Requires liquid flow rate and transport efficiency
ES-DMA-CPC	N	Number of events	Restricted by nebulisation (electrospray) of particles Requires nebulisation efficiency calibration
DCS	N	Sedimentation rate	Restricted to particles of known shape Requires physical density and refractive index

DLS	N	Scattered light intensity and fluctuations	Restricted to monodisperse spherical particles Requires refractive index
PTA	Y	Particle movement	Restricted to dilute particles Requires calibration of analysed volume
UV-vis	N	Extinction of light	Easily applicable only to monodisperse particles Requires particle size and shape

#### 4.1.2 Samples

A set of monodisperse spherical particle samples were obtained. A list of samples is provided in **Table 2**. Particles of smaller and larger sizes were also analysed, but because of the limitations of sample stability and the limited range of techniques able to accurately measure concentrations only those suitable for a broad-ranging intercomparison are listed. The nominal diameters and concentrations are listed in the table. The nominal concentrations are based upon gravimetric measurements and various assumptions about the size, shape, insolubility of the particles and the absence of other non-volatile materials.

Both gold and polystyrene particles proved useful as reference materials. Silica particles also provided useful results, but significant uncertainties arose for two reasons: firstly, the silica particles existed in equilibrium with dissolved silicic acid and secondly, the density of the particles was lower than expected ( $1.9 \text{ g cm}^{-3}$ , rather than the assumed  $2.2 \text{ g cm}^{-3}$ ). Dissolved silicon resulted in a poor detection limit for particles in spICPMS and therefore the accuracy of number concentration measurements relies upon SAXS measurements for which material density is an important parameter. For these particles, accurate number concentrations could only be established within a factor of two.

##### *Gold particles*

Citrate stabilised gold nanoparticles with nominal size of 5 nm, 10 nm, 30 nm, 100 nm, 250 nm and 500 nm were purchased from BBI International (Cardiff, UK). The nominal concentration of the particle in solution declared by the manufacturer is reported in Table 2. Where possible, the particles were analysed as purchased. If dilution was required, this was performed gravimetrically by using 1 mM citrate buffer as a dispersion medium.

##### *Polystyrene particles*

Polystyrene nanoparticles were synthesized by emulsion polymerization of styrene using sodium dodecyl sulphate (SDS) as surfactant. The polymerization reactions were carried out in a 1 l five-neck reactor equipped with a condenser, a mechanical stirrer, a thermometer and inlets for nitrogen and styrene. 500 ml of ultrapure water containing 0.3 g SDS were introduced into the reactor at room temperature with a stirring rate of 300 rpm, and 50 ml of styrene was added dropwise. The mixture was purged with nitrogen, and nitrogen was fluxed during the entire polymerization procedure. The reactor was heated to  $80^\circ\text{C}$ , a potassium persulfate aqueous solution (5.0 ml, 0.74 mmol) was added, and the mixture was reacted for 24 h. The obtained latex was purified from surfactant and unreacted monomer by repeated dialyses against ultrapure water (cellulose membrane, molecular weight cut-off 12 kDa).

##### *Silica particles*

Silica nanoparticles were produced by tetraethylorthosilicate hydrolysis in an oil/water system. The particles were produced during a single nucleation event under constant temperature. After the synthesis was complete, the solvent was exchanged for water without centrifugation or drying by tangential ultra-filtration. After cleaning the suspension had a content of less than 0.6 % ethanol.

**Table 2:** List of particles used in Innanopart for comparison of concentration measurements.

Material	Supplier	Nominal Diameters (nm)	Nominal Concentration (Particles mL <sup>-1</sup> )
Gold	NPL	5; 10; 30; 100; 250; 500	$5.0 \cdot 10^{13}$ ; $5.7 \cdot 10^{12}$ ; $2.0 \cdot 10^{11}$ ; $5.6 \cdot 10^9$ ; $3.6 \cdot 10^8$ ; $4.6 \cdot 10^7$
Polystyrene Set 1	UPO	60; 120; 200; 250; 300	$8.4 \cdot 10^{14}$ ; $8.3 \cdot 10^{13}$ ; $2.9 \cdot 10^{13}$ ; $1.4 \cdot 10^{13}$ ; $2.5 \cdot 10^{12}$
Polystyrene Set 2	UPO	65; 80; 170; 245	$4.0 \cdot 10^{14}$ ; $1.3 \cdot 10^{14}$ ; $1.5 \cdot 10^{13}$ ; $7.0 \cdot 10^{12}$
Silica	CEA	20; 45; 100	$1.8 \cdot 10^{14}$ ; $4.7 \cdot 10^{13}$ ; $4.0 \cdot 10^{12}$

### 4.1.3 Development of Accurate Methods

#### *Small angle X-ray Scattering (SAXS)*

SAXS measurements were performed at four-crystal monochromator beamline (FCM) of PTB with the SAXS setup at the BESSY II synchrotron radiation facility (Helmholtz-Zentrum Berlin) at the fixed photon energy of 8000(8) eV. The samples were filled in vacuum-proof borosilicate glass capillaries with length of 80.0 mm, width of 4.2 mm and total thickness of 1.25 mm. These capillaries produced by Hilgenberg (Malsfeld, Germany) have a wall thickness of 120  $\mu\text{m}$ . The capillaries were sealed. The lower section was filled with Fluorinert FC-3283, acquired from Iolitec (Heilbronn, Germany), which has a density of  $1.82 \text{ g cm}^{-3}$ , low viscosity and is immiscible with aqueous solutions. With help of a calibration liquid the sample thickness was determined traceably. The capillaries were scanned with step size 0.5 mm to ensure that there was no sedimentation during the experiment, as in this case the concentration at all heights would be the same. At each point a scattering pattern was obtained with exposure time 60 s. The scattering pattern were collected with Pilatus 1M detector (Dectris Ltd., Baden, Switzerland). The measured intensity was normalised to the quantum efficiency of the detector at the given energy of 8000 eV. The transmitted photon flux was measured with and without sample to access the sample transmittance order to calculate the sample thickness. The incoming flux was measured using a calibrated silicon diode. The distance between detector and the sample was 4511(5) mm. All scattering curves obtained from the data were normalized to the total transmission of sample and the capillary.

As the concentration measurements have to be traceable a determination of the uncertainty budget for the experiment is of vital importance. The uncertainty of all normalisation values has to be accounted for. The complete list of the contributions is listed in **Table 3** for a 30 nm gold nanoparticle sample. For the calculation of the contrast a gold density of  $19.3(5) \text{ g/cm}^3$  was used. Here, we can see that the major contributor to the uncertainty in the final concentration is the uncertainty in electron density. In the case of gold, this is estimated from literature data, but for organic materials can be directly measured by changing the electron density of the suspension medium and observing the effect on the scattered intensity. When the scattered intensity is minimised, the electron density of the suspension medium is the same as that of the sample. For PS particles this was the approach that was taken, however for silica particles it was not possible to find suspension media which were sufficiently dense to use this approach. In that case, estimates again were made based upon the physically measured density using DCS.

**Table 3:** Uncertainty budget for an example SAXS measurement.

Parameter	Value	Uncertainty in Value	Contribution to the final uncertainty $U_c / \text{cm}^3$
Photon energy	8000.0 eV	0.8 eV	$5.6 \cdot 10^8$
Detector pixel size	172.1 $\mu\text{m}$	0.2 $\mu\text{m}$	$6.1 \cdot 10^9$
Distance to detector	4511 mm	5 mm	$5.7 \cdot 10^9$
Source intensity	$6.8 \cdot 10^9 \text{ ph s}^{-1}$	$6.8 \cdot 10^7 \text{ ph s}^{-1}$	$1.9 \cdot 10^9$
Sample transmittance	2.00 %	0.02 %	$1.9 \cdot 10^9$
Acquisition time	60.00 s	0.06 s	$1.9 \cdot 10^9$
Detector efficiency	97 %	3 %	$6.0 \cdot 10^7$
Sample thickness	1.01 mm	0.03 mm	$6.0 \cdot 10^8$
Fitting	$2.75 \cdot 10^{-5}$	$9.0 \cdot 10^{-7}$	$4.4 \cdot 10^9$
Electron density contrast	$4340 \text{ nm}^{-3}$	$120 \text{ nm}^{-3}$	$1.0 \cdot 10^{10}$
<b>Concentration, C</b>	<b><math>1.85 \cdot 10^{11} \text{ cm}^{-3}</math></b>	<b><math>1.3 \cdot 10^{10}</math></b>	<b>NA</b>

#### Single particle inductively coupled plasma mass spectrometry (spICPMS)

Single particle Inductively Coupled Plasma Mass Spectrometry (spICPMS) is a recently emerged method, allowing particle number-based concentration measurements. The approach was originally developed by Degueldre *et al.* In spICPMS, sample needs to be diluted to a concentration in the range of ng/kg and is then introduced into the ICPMS instrument at a known mass flow rate. The technique works by acquiring individual intensity readings with very short dwell times (in the milliseconds range and more recently, with advances in instrumentation, in the microsecond range). The sum of acquired pulses representing individual particles is directly proportional to the particle number-based concentration in the sample, which can be calculated from **Equation 1**:

$$C(\text{NP/kg}) = \frac{N \cdot D_f \cdot 1000}{\eta \cdot V} \quad [1]$$

where  $N$  is the number of particles detected in time scan ( $\text{min}^{-1}$ ),  $D_f$  is the sample dilution factor of the samples,  $\eta$  is the transport efficiency and  $V$  is the sample mass flow ( $\text{g/min}$ ).

The transport efficiency ( $\eta$ ) here was determined using a revisited and novel waste collection method developed in this project. This approach allows direct traceability to the SI unit of kilogram and the unit 1 (particle counting). In this approach the sample uptake flow rate and the nebuliser flow rate are measured gravimetrically over 15 and 45 min time respectively, ensuring the instrument reaches the steady state conditions before measurements. The transport efficiency ( $\eta$ ) was then calculated as the ratio of the nebuliser flow rate to the sample flow rate.

SpICPMS measurements were performed using an 8900 ICPMS instrument manufactured by Agilent Technologies. The instrument was equipped with the MassHunter4.3 (version: G72dC C.01.03) software and microsecond detection capability, allowing analysis in a single particle mode. After verifying the instrument's performance with 1  $\mu\text{g/kg}$  Agilent Tuning solution, the ICPMS conditions were optimised to obtain maximum  $^{197}\text{Au}$  sensitivity with a minimum background contribution using 1  $\mu\text{g/kg}$  ionic gold solution (SRM 3121 NIST). Analyses in fast transient analysis (TRA) mode were performed with 'No Gas' using a dwell time of 0.1 ms per point, with no settling time between the measurements and using the newly developed Single Particle Application Module of the ICPMS MassHunter software (G5714A). The instrument was cleaned with 1 % (v/v) Aqua Regia solution followed by ultrapure water after each sample. Each sample was measured 5 times under repeatability conditions.

Using spICPMS, it was possible to detect gold particles as small as 10 nm, but not to measure their number concentration reliably. Particles of around 30 nm, 100 nm and 250 nm were all suitable for the technique. However, a secondary population of particles was found in the sample of 250 nm gold making it unsuitable for the use as a reference (test) material. The largest, 500 nm gold particles appeared to sediment before the measurements could be performed. Smaller silica particles (20 and 50 nm) were not detected with the instrumental set-up used due to the high background due to particle dissolution.

The summary of the accurate spICPMS particle concentration values are shown in **Table 4**. The values represent particle concentration in the original samples, derived using the Equation 2. Reported particle concentration values equate to 95.2 – 102.2% recovery rates for 30 – 100 nm gold samples (Note: recovery rate here is relative to the expected particle number calculated from the total element content quantified and TEM size supplied by the material manufacturer or in case of 8013 NIST taken from the certification report). Particle number-based concentration values obtained with the revisited waste collection method reported here were also in a very good agreement (within the measurement uncertainty) with values obtained with the particle frequency approach, described in PD ISO/TS 19590:2017, using 8013 NIST for the nebulisation efficiency ( $\eta$ ) determination, **Table 5**.

**Table 4** Particle number-based concentration values measured with spICPMS.

Sample	NP concentration [NP/kg]	Standard Uncertainty [NP/kg]	Expanded uncertainty at 95% confidence interval, k=2 [NP/kg]	Relative expanded uncertainty [%]
30 nm gold	$1.80 \cdot 10^{14}$	$6.84 \cdot 10^{12}$	$1.37 \cdot 10^{13}$	7.6
60 nm gold 8013 NIST	$2.76 \cdot 10^{13}$	$8.69 \cdot 10^{11}$	$1.74 \cdot 10^{12}$	6.3
100 nm gold	$4.10 \cdot 10^{12}$	$1.30 \cdot 10^{11}$	$2.60 \cdot 10^{11}$	6.3

**Table 5.** Particle number-based concentrations values with spICPMS following the revisited waste collection and particle frequency approaches, shown as mean  $\pm$  expanded uncertainty, k=2 (relative expanded uncertainty quoted in the brackets).

Sample	Particle number-based concentration	
	Mean $\pm$ U, k=2 [NP/kg]	
	Revisited waste collection method	Particle frequency method
30 nm gold	$(1.80 \pm 0.14) \cdot 10^{14}$ (7.6%)	$(1.90 \pm 0.24) \cdot 10^{14}$ (12.4%)
60 nm gold 8013 NIST	$(2.76 \pm 0.17) \cdot 10^{13}$ (6.3%)	$(2.91 \pm 0.26) \cdot 10^{13}$ (8.8%)
100 nm gold	$(4.10 \pm 0.26) \cdot 10^{12}$ (6.3%)	$(4.38 \pm 0.33) \cdot 10^{12}$ (7.5%)

In order to calculate the measurement uncertainty associated with particle number determination with the revisited waste collection approach, the individual uncertainty components associated with the number of particles detected in time scan ( $N$ ), sample dilution factor ( $D_f$ ), transport efficiency ( $\eta$ ) and the sample mass flow ( $V$ ) were estimated and combined in accordance with ISO 17025 and Eurachem/CITAC guidelines. Coverage factor k=2 was used to calculate the expanded uncertainty at 95% confidence interval, whilst the relative expanded uncertainties ( $\% \text{ NP} \cdot \text{kg}^{-1} / \text{NP} \cdot \text{kg}^{-1}$ ) were derived by dividing the expanded uncertainty value by the average particle concentration value and multiplying by a factor of 100. The summary of the obtained results is shown in **Table 4**, whilst the contribution (% total) of the individual components in the overall uncertainty is shown in **Table 6**.

**Table 6.** Typical uncertainty budget.

Sample	Uncertainty contribution (%)			
	Number of particles detected in time scan	Dilution factor	Transport efficiency	Sample mass flow
30 nm gold	74.1	14.1	11.0	0.8
60 nm gold 8013 NIST	76.4	3.2	18.0	2.4
100 nm gold	71.4	4.3	20.2	4.2

*UV-visible spectroscopy (UV-vis)*

The extinction of light passing through a colloid can be measured in a UV-visible spectrometer operating as a turbidimeter. For spherical particles of known refractive index and under the assumption of single scattering, the results can be directly compared to light scattering theory. For gold particles, the spectra also provide information about the size and shape of particles due to resonant absorptions caused by surface plasmons. Spherical, monodisperse gold particles have been particularly well studied with literature methods for number concentration available and these methods were used. The estimated relative uncertainty using UV-vis is approximately 20 % and is dominated by the uncertainty in refractive index of gold and the surrounding media and the effect of the shape of gold particles. In the initial stages of the project, the uncertainties of this method were sufficiently large for it to be considered a laboratory method rather than an accurate method. However, as the project developed it became clear that for gold particles it was a useful, robust and accurate method with uncertainty comparable to the other accurate methods and applicable to a wider range of sizes. Therefore, it is included in this section. The current literature provides simple methods for converting light absorption into number concentration for gold particles in the range 1 nm to 100 nm diameter. Within the project, this range was extended to 1000 nm diameter using Mie scattering theory and the effect of particle aggregation was considered using the T-matrix superposition method. **Figure 1(a)** demonstrates the general sensitivity of UV-vis spectroscopy to the shape of gold nanoparticles, but also indicates the low wavelength region (\*) which is insensitive to these effects and can be used, as a first approximation to measure the mass concentration of gold. For monodispersed particles, the diameter can be obtained from the position of the single plasmonic peak in the spectrum, aggregated particles defy simple analysis as described later. **Figure 1(b)** demonstrates the manner in which the extinction efficiency,  $Q_{ext}$ , in the quantitative region changes as a function of diameter (note that the diameter axis is on a logarithmic scale). Below 100 nm diameter, the literature method is validated by these calculations. Above 100 nm the effect of particle shape becomes important, with ~16 % discrepancy between spheres and doublets as expected from cross sectional area considerations. The thin line through the values for spheres is **Equation [2]** developed in the project, the line marked Haiss *et al* is the literature curve (a Gaussian) valid below 100 nm. This relationship is as accurate as the Haiss *et al* below 100 nm and has the advantage of being useful for larger particles.

$$Q_{ext} = \frac{3.45}{\left[ \left( \frac{D}{72.5} + \left\{ \frac{D}{60.4} \right\}^4 \right)^{-1.2} + \left( \frac{D}{72.5} \right)^{0.12} \right]} \quad [2]$$

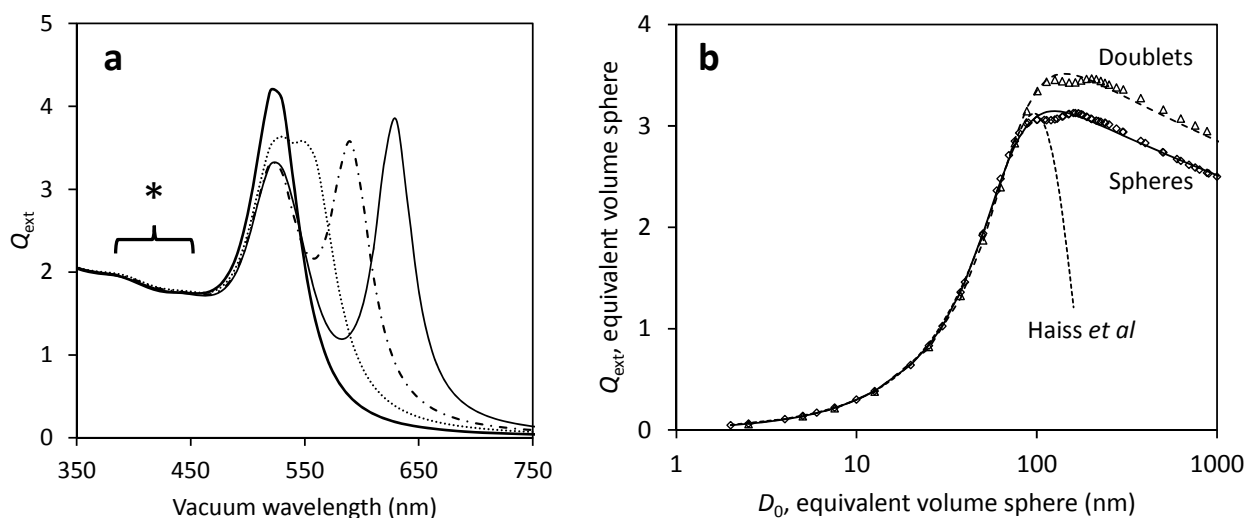


**Figure 1:** Calculated extinction efficiencies,  $Q_{\text{ext}}$ , for gold nanoparticles in water. (a) 40 nm diameter spherical gold particles, bold line represents twice the value for monodisperse particles, the other lines are doublet particles with interparticle separations of 1 nm, 2 nm and 5 nm. The region marked with a star is used for quantitative analysis. (b) Quantitative region as a function of particle size for spheres and doublets. Lines following the data are descriptions developed in the Innanopart project and the literature description is marked „Haiss *et al.*“.

#### 4.1.4 Comparison with Laboratory Methods

The particles listed in **Table 2** were analysed in this project using methods that are commonly used in industrial and academic laboratories. A brief summary of each of the methods is provided below. Note that many of the techniques operate in a defined range of particle concentrations and the samples required dilution in some cases. In the project, particle providers were tasked with developing storage, handling and dilution protocols and assessing the stability of the particles over several months to ensure comparability between methods. For all of the techniques listed an assessment of the linearity and detection limits were made using these particles and dilution protocols.

##### **Population average methods**

###### *Dynamic Light Scattering (DLS)*

DLS measures light scattered by particles at a fixed angle. The rate of fluctuations in the scattered light permits an assessment of the rate of diffusion of particles, and therefore their size. The method is primarily used to measure particle size and can measure particles over a wide range of size, material and concentration. Hence, it is widespread. For monodispersed, spherical particles it is known to provide accurate size measurements and, in this case, the absolute intensity of the scattered light can be converted into a number concentration, provided that the refractive index of the particles and dispersion medium are known. The software associated with the instrument used (Malvern Zetasizer Nano ZS 3600) converts the scattered intensity into volume concentration and the measured particle size is then used to generate a number concentration.

###### *Differential Centrifugal Sedimentation (DCS)*

Centrifugal sedimentation provides a highly precise separation of particles. The sedimentation rate depends upon the size, shape and density of the particle population, and the relationships are well understood. In DCS, the particles are injected into a liquid medium in a centrifuge and their sedimentation rate measured by the time taken to reach a detection position. Detection is normally performed through turbidimetry and the mass concentration measured through light scattering theory under the assumption of single scattering. Number concentration can be inferred from the measured particle diameter. The physical densities and refractive indexes of both the particles and the liquid are required. In the project, the software provided by the manufacturer (CPS Instruments Inc.) was employed, but was also independently validated using raw data output from the instrument.

#### *Hollow Core – Photonic Crystal Fibre (HC-PCF)*

Particles are loaded into a capillary at the centre of a photonic crystal fibre which acts as a waveguide for light. The waveguide then permits significantly enhanced interaction between the suspension and light with an anticipated increase in sensitivity. The particles are detected either through light extinction or through emission. For the particles tested here, gold particles were analysed through light absorption and polystyrene through the detection of Raman scattered light. Within Innanopart, it was shown that effective loading of the capillary was a significant challenge and only some polystyrene particles could be detected using this method.

#### **Particle counting methods**

##### *Particle Tracking Analysis (PTA)*

PTA operates by directly observing the light scattered by individual particles. It operates in the very dilute regime where particles are separated in space sufficiently to be resolved from each other, analysis of their Brownian motion provides their hydrodynamic diameter and the number concentration is found by simply counting the particles and dividing by the volume in the field of view. The volume has well defined lateral extent, but is hard to define in depth due to the overlapping light intensity distribution and depth of focus of the microscope used. This depth of field may also change with the light scattering properties of the particle, *i.e.* chemistry, size and shape. The manufacturers provide software for this purpose and one of these (Malvern NTA3.2) was used in the project.

Since, PTA relies on detecting the light scattered by particles, the size limit of detection is largely dependent on the type of material the particles are composed of. For strongly scattering gold, the lower size limit of detection was found in the range of 10 nm, but for particles composed of silica, the lower size limit of detection increased to around 40 nm. The upper size limit of detection is restricted by particles sedimenting out of the field of view. Particles of higher density *e.g.* gold will sediment easier than *e.g.* polystyrene, meaning that gold particles of 500 nm in diameter could not be detected, whilst polystyrene particles with diameter larger than 500 nm were quantified reliably. Within the size limits of detection, the technique was found linear for all tested materials.

##### *Tunable Resistive Pulse Sensing (TRPS)*

In TRPS, two volumes of liquid containing an electrolyte are separated by a small aperture. A potential difference is established between the two volumes and the current through the aperture monitored. When a particle traverses the aperture a drop in current is observed and the size of the particle inferred from the magnitude of this blockade event. The frequency of events is directly related to particle concentration and independent of particle size and material, provided that the particles are detectable. Effects such as electro-osmosis and pressure differences need to be taken into account, either through calibrant particles or through a series of experiments using different instrumental settings. Data was analysed using the software provided by the manufacturer (Izon Science Ltd.).

##### *Electrospray – Differential Mobility Analysis – Condensation Particle Counter (ES-DMA-CPC)*

A flow of suspended particles is aerosolised using an electrospray and, after solvent evaporation, is size selected using an electrostatic mobility analyser. The particles are then detected by introducing them into a saturated organic vapour where they nucleate the growth of a liquid drop. Particles that have passed through the whole system are counted using optical detection. The method has an unknown efficiency and the purpose of this work was to establish the transmission efficiency, whether it was material dependent and which experimental factors influenced the results. In the following, the number of detected particles are reported, but the important findings of the project are that the electrospray transmission efficiency varies from ~10 % to ~80 % and depends strongly upon the sample matrix (*e.g.* solvent type and sample conductivity) and possibly upon the type of particle. Efficiency is improved at low sample flow rates. Moreover, methods to reduce interferences from non-volatile solutes were demonstrated. The ES-DMA-CPC method is suitable for samples with NP size ranging between a few nm up to 1  $\mu\text{m}$  in a concentration range between  $\sim 10^9 \text{ cm}^{-3}$  and  $\sim 10^{13} \text{ cm}^{-3}$ . Higher concentrations should be avoided as particle aggregation may be induced upon aerosolisation of the suspension.

#### **4.1.5 Summary of results**

##### *Gold particles*

Accurate methods were used to establish number concentrations for a range of particles from 5 nm to 500 nm in diameter. For these, there is sufficient literature on the use of UV-vis spectroscopy to provide a comparison to de facto standard methods which are widely employed up to 100 nm diameter. SAXS, in the set up

implemented within this project, had an upper size limit of less than 100 nm for gold particles due to sedimentation which altered the concentration in the analysis region. For spICPMS, the sensitivity was insufficient to reliably detect the 10 nm particles and, therefore, the common reference point for accurate methods was the 30 nm gold particle sample. It is therefore appropriate to compare all analyses to UV-vis, because of its applicability to all samples, provided that the results from SAXS and spICPMS validate the UV-vis spectroscopy results for the samples where comparison is possible.

**Figure 2(a)** illustrates the number concentration of gold particles determined by UV-vis in the full range of samples (5 nm to 500 nm). For comparison, the red dashed line shows the inverse cubic relationship expected if all samples contain the same mass concentration of gold. **Figure 2(b)** compares the three accurate methods for the 10 nm, 30 nm and 100 nm gold particles. Here, the agreement between methods is within 10% and the relative uncertainty of spICPMS has been improved to better than 10%, indicating that the UV-vis results appear to overestimate concentrations by approximately 5%. These results independently validate the de facto standard method of UV-vis spectroscopy for gold nanoparticle concentration. **Figure 2(c)** compares the results of laboratory methods with the concentrations determined by UV-vis spectroscopy. PTA analysis for the 30 nm and 100 nm samples provided results that were within 5% of the accurate methods. DCS analysis was within a factor of two of the UV-vis concentrations and demonstrated a trend of increasingly underestimating the concentration of particles as the diameter increased. The causes of this underestimation are unclear despite a detailed study of the physical principles and operation of the method. The detection wavelength, 405 nm, is consistent with the quantitative region of the gold absorption spectrum described in the UV-vis section, therefore the mass of gold particles injected should be correctly measured. The ES-DMA-CPC underestimates particle concentrations by a factor of approximately 10, which is expected because of losses during the nebulisation and transport processes. The purpose in this study is to establish the magnitude of such losses and to measure the efficiency of the method for colloidal nanoparticles. It is also possible to calibrate the detection efficiency using these reference particles, as described later in **section 4.1.6**.

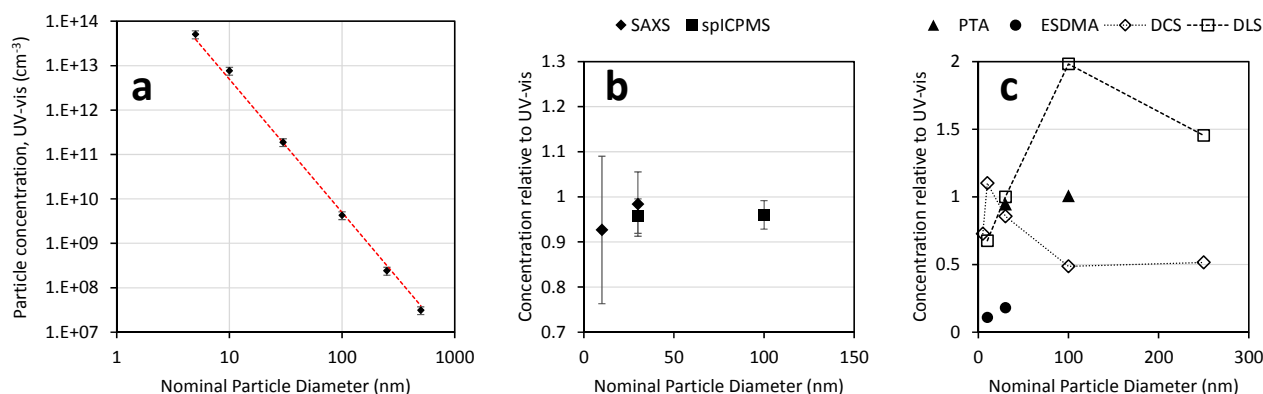


**Figure 2:** Particle number concentrations of gold reference materials used in Innanopart. (a) UV-vis concentrations for all samples plotted on log-log axes, error bars represent 20 % relative uncertainty. The dashed red line represents a constant  $0.051 \text{ mg/cm}^3$  gold mass concentration. (b) Accurate methods compared to UV-vis, error bars are rigorously calculated uncertainties. (c) Laboratory methods compared to UV-vis.

These results demonstrate that it is possible to accurately measure the number concentration of monodisperse gold particles through SAXS, spICPMS, UV-vis and PTA. These findings were presented at a dedicated workshop on the topic organised by LGC and NPL at BIPM-CCQM and jointly held between the Inorganic Analysis Working Group (IAWG) and the Surface Analysis Working Group (SAWG). Following the workshop, the first international pilot study on the accurate measurement of concentration of colloidal gold particles, organised by LGC, is being carried out amongst National Measurement Institutes. This is consecutive with a similar study for academic and industrial laboratories organised by NPL under the auspices of VAMAS TWA 34 (Nanoparticle Populations) with nearly 50 laboratories involved, making it one of the largest studies carried out in VAMAS.

#### Polystyrene particles

Two polystyrene series were measured as the first batch of the first series showed instabilities. However, not all facilities could measure the second series.

The results for the first PS-series were provided by SAXS, PTA, DLS, DCS, ES-DMA-CPC. For most samples the SAXS results were not consistent with the other methods, typically being a factor of 3 lower with a high

level of scatter. However, comparison between the other methods and the nominal concentrations showed better absolute agreement and reasonable linearity. Therefore it was concluded that the SAXS samples had been compromised in some way. It also became clear that the uncertainty for polystyrene measurements is higher for SAXS, as the electron density contrast between water and PS is low. The contrast in this experiment was improved by diluting water with ethanol 1:1. For gold particles the uncertainty was below 10 %, but for PS particles in water it is close to 80 %. With dilution in ethanol the uncertainty from electron density contrast drops below 20 %. Therefore a second set of samples were requested with PS in an ethanol-water mix.

The results of the second PS-series were provided by SAXS, DLS, DCS, TRPS, ES-DMA-CPC and HC-PCF. Only SAXS, DCS and DLS delivered results for all samples. For the second PS series, which also had to be diluted in ethanol, SAXS provided an uncertainty of 15 %. The results of the DCS method match the results of the SAXS most closely for the large particles. For the sample PS245 all the provided concentrations except DLS agree within given uncertainties. For all other samples the results of these two methods are still closest. The only number provided by ES-DMA-CPC for PS170 is factor 2 apart from the number obtained by SAXS and DCS. The results for sample PS80 from TRPS and DCS are approximately factor 2 apart from the primary method, while DLS is very close. For PS60 DLS is within the range of the reference method, while DCS shows a factor 3 difference.

#### *Silica particles:*

For silica samples only SAXS, DLS, DCS and ES-DMA-CPC delivered final results. The measurements with spICPMS identified particle dissolution for these samples. Therefore PTA could only deliver a result for the 100 nm diameter sample. Possible dissolution and respective more than one population of the particles as well as connected density changes affect results obtained by SAXS and DCS. A measurement of silica density delivered a value of  $\rho = 1.89(4) \text{ g/cm}^3$  instead of the first assumed  $\rho = 2.2(1) \text{ g/cm}^3$ . The lower density results in the higher number concentration by a factor of  $\sim 2$  on the SAXS values. For the sample of 20 nm diameter only SAXS delivered number concentrations, which could only be compared with the nominal concentration. For the 45 nm diameter sample the results do not agree well within their uncertainties and show variation up to factor 10. The nominal concentration agrees well with the concentration measured by SAXS as density  $\rho = 2.2(1) \text{ g/cm}^3$  was assumed, as the nominal value measures all the mass of silica in sample - particles and dissolved content. Other methods deviate from this value - concentration calculated by SAXS with  $\rho = 1.89(4) \text{ g/cm}^3$  is higher as the results from ES-DMA-CPC, DLS and DCS are lower. However, it is unclear how the change in density will affect the refractive index of the particles and this is a critically important parameter for DLS and DCS. The results for the largest silica particles agree better with maximal deviation of factor 5. Within the determined uncertainties PTA and nominal results are compatible with the results from SAXS at  $\rho = 1.89(4) \text{ g/cm}^3$  for the 100 nm diameter sample. DLS results are within the range of the DCS results, as well as SAXS results for  $\rho = 2.2(1) \text{ g/cm}^3$ . The high deviations of the laboratory methods from primary method might be due to dissolution of silica particles and change of density, because of that dissolution. It is possible that the larger the particles are the smaller the influence the dissolution and therefore the results for largest silica particles agree better.

Therefore, the silica particles proved not to be useful as a reference material due to the large uncertainties and variable results. These results demonstrate the critical need for better reference data and for experiments to confirm assumptions made in the calculation of concentration.

#### **4.1.6 Mixed Particle Populations**

The ability of the various techniques to measure the concentration of mixed nanoparticle samples was tested using a set of samples containing a binary mixture of particles differing in materials, size and concentration **Table 7**. Many of the observations discussed in section 4.1.5 also apply here, therefore we will concentrate here on the performance of the techniques in relation to their ability to discriminate and measure particles in mixtures.

**Table 4.1.7:** List of particle mixtures used in Innanopart for comparison of concentration measurements. A tick indicates the component was detected, while a cross indicates that it was not. Dashes indicate the experiment was not performed. \*Requires reference data for individual components.

	Components	Concentration (nominal, cm <sup>-3</sup> )	UV-Vis*	SAXS	DCS	DLS	PTA	spICPMS	ESDMA
Mix 1	10 nm gold	2.85·10 <sup>12</sup>	✓	✓	✓	✗	---	✓	✓
	30 nm gold	1.00·10 <sup>11</sup>	✓	✓	✓	✓	---	✓	✓
Mix 2	10 nm gold	2.85·10 <sup>12</sup>	✓	✓	✓	✗	---	✓	---
	100 nm gold	2.80·10 <sup>9</sup>	✓	✓	✓	✓	---	✓	---
Mix 3	100 nm silica	3.67·10 <sup>11</sup>	✓	✗	✓	✗	✓	✗	---
	100 nm gold	3.73·10 <sup>9</sup>	✓	✗	✓	✓	✗	✓	---
Mix 4	100 nm silica	3.67·10 <sup>11</sup>	---	✗	✓	✓	✓	---	---
	300 nm PS	3.95·10 <sup>8</sup>	---	✗	✓	✗	✗	---	---
Mix 5	10 nm gold	1.97·10 <sup>11</sup>	✓	✗	✓	✗	---	✓	---
	30 nm gold	1.93·10 <sup>11</sup>	✓	✗	✓	✓	---	✓	---
Mix 6	10 nm gold	5.69·10 <sup>9</sup>	✓	✓	✗	✗	---	✓	---
	100 nm gold	5.59·10 <sup>9</sup>	✓	✓	✓	✓	---	✓	---
Mix 7	100 nm silica	5.47·10 <sup>9</sup>	✓	✓	✓	✗	✓	✗	---
	100 nm gold	5.57·10 <sup>9</sup>	✓	✓	✓	✓	✓	✓	---
Mix 8	100 nm silica	8.05·10 <sup>10</sup>	---	✓	✗	✓	✓	---	---
	300 nm PS	7.94·10 <sup>10</sup>	---	✓	✓	✓	✓	---	---

Not every technique could measure all the samples. For example, samples containing polystyrene were not measured by spICPMS, and samples containing nanoparticles below 50 nm were not measured by PTA. UV-Vis was used to quantify the composition of the samples containing gold nanoparticles only. For UV-vis, the spectra of the particle mixtures were fitted with a linear combination of reference spectra taken from the single components, which were independently acquired. The measurement results for a number of methods are shown in **Figure 3**. Among the ensemble techniques (**Figure 3a-c**), SAXS delivered relatively accurate measurements results for gold nanoparticles, despite the challenges faced in the data analysis due to the relatively complicated model that was required to fit the scattering data. When samples differed in both materials and size, the modelling of the scattering curve is extremely challenging without some knowledge of the sample composition. This is reflected in the relatively low accuracy and high uncertainties associated to the measurement results. DLS delivered reasonable results considering that the instrument used is not designed for the measurement of particle concentration. However, generally only the particle population of the mixture with the highest total scattered intensity was detected. DCS was capable of measuring most particle populations. As the time of sedimentation measured by the technique depends on the density, as well as the size of the particles, high resolution size distributions could be measured also for samples mixed with particles of similar size but different materials. However, DCS consistently underestimated the concentration of these particles, as observed also in section 4.1.5.

Particle by particle techniques delivered more accurate results than the ensemble methods (**Figure 3d-f**). PTA was able to differentiate populations by size and materials, owing to its high size resolution and the different intensity of the light scattered by particles of different materials. The measurement of particle populations differing significantly in concentration was challenging, due to the narrow window of concentrations accepted during the measurements. This window is generally reached by dilution of the sample, which can be optimised only for the most concentrated of the mixture components. Dilution is also a problem for spICPMS, but here this was solved by measuring each mixture at different sample dilutions and selecting the measurement results

that provided the most accurate particle diameters. ES-DMA-CPC could measure only one sample of sufficiently high concentration for the technique. The high resolution of the technique allowed discrimination of the 10 nm from the 30 nm nanoparticles and the measurement of their concentration with accuracy. Here, calibration of the transport and detection efficiencies for each particle was required as described in **section 4.1.5**.

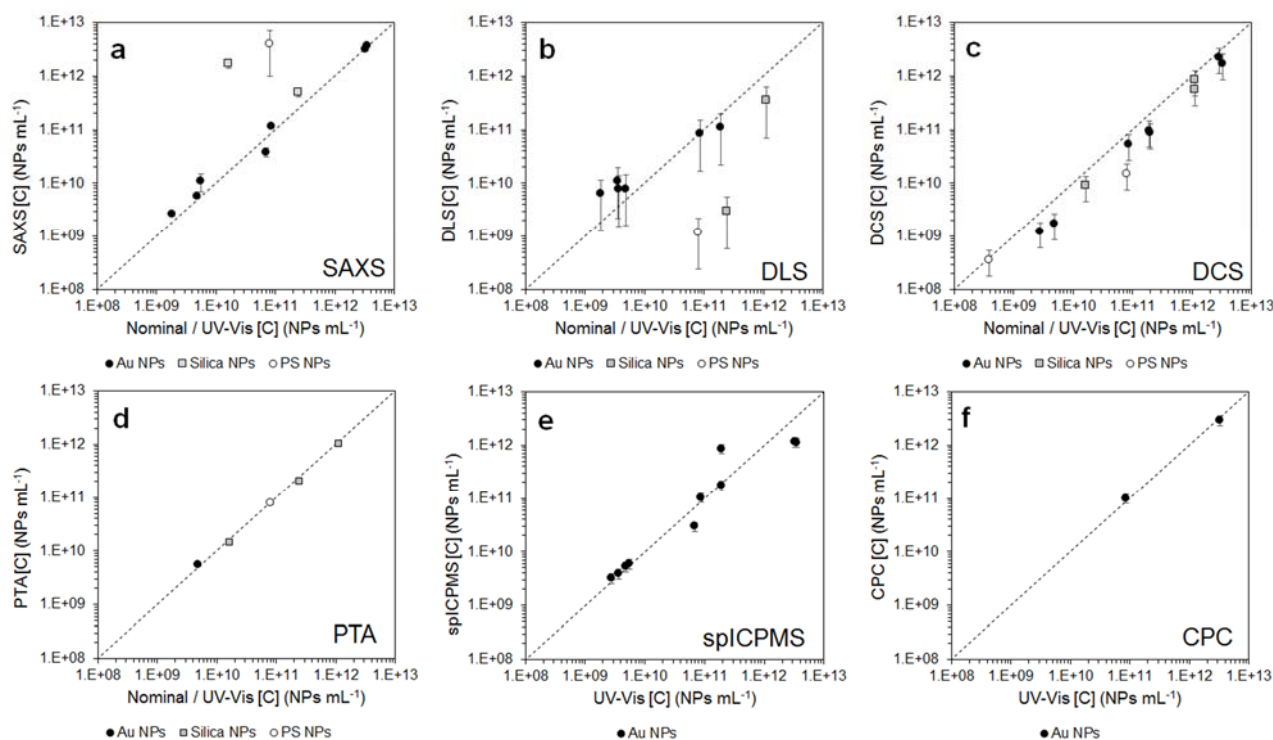


**Figure 4.1.3:** Particle number concentrations of mixed samples materials used in Innanopart plotted on log-log axes relative to the nominal concentration or the concentration measured by UV-Vis (for gold nanoparticles). Results for (a) SAXS; (b) DLS; (c) DCS; (d) PTA; (e) spICPMS and (f) ES-DMA-CPC.

#### 4.1.7 Aggregated and non-spherical Particle Populations

When measuring nanoparticle concentration, it is important to understand the contribution that agglomerates or aggregates make to bias the measured values, since some methods will count agglomerates as one particle, others as many particles and only a few techniques have the size resolution to resolve them from the primary particle population. Aggregated particles are non-spherical and therefore a general method to measure non-spherical particles is encapsulated in these results. In **Table 8**, the techniques considered in the project are compared and classified. Some methods measure particles as an ensemble and others particle-by-particle. The latter are more likely to be able to identify aggregated particles, although in all cases an aggregate will count as an individual particle. The effect of aggregation or non-sphericity on ensemble methods is more difficult to evaluate. SAXS is sensitive to short range order in the sample and the scattering curve for an aggregate will largely resemble that of an equivalent monodisperse sample except for the scattering at very small angles, the Guinier region, where the effect of inter-particle separation should be evident. For methods that are unable to distinguish primary particles from aggregates, the aggregate will increase the measured average size of the population. It is then a question of whether this average size is appropriate for the calculation of particle concentration.

For some ensemble methods, such as DCS, the various sub-populations of agglomerates are separable, provided that the sample is reasonably monodisperse (<10 % relative variation in diameter). Thus, these methods could be used to obtain the *relative* concentrations of different states of aggregation, provided that the measurements of concentration within each sub-population were consistent. For DCS, this involves understanding the effect of particle shape on both sedimentation time and light extinction. Whilst the first effect is well documented, and directly measurable, the second involves detailed calculations. In this project we used a relevant T-matrix superposition method code available from a NASA website in Fortran. This was translated

into the more widely used MATLAB code and made publicly available in the supplementary information in one of our papers [paper 9] and used, for example to generate the data shown in Table 9. Detailed calculations showed that for DCS the error in the *relative* concentrations monomeric to dimeric particles remains below 20 % in all reasonable situations even with a naïve interpretation. For gold particles, using suitable wavelengths for detection in the quantitative region of 400 nm to 450 nm, the error in relative mass concentrations will be better than 10 %. Provided that a suitable correction is made for the error in size resulting from particle shape, the *relative* number concentration will have a similar error.

**Table 8.** Characteristics of the laboratory methods in the presence of agglomeration.

Technique	Type of method	Sample concentration	Agglomerate interpretation	Impact of spherical approximation
DCS	Ensemble	Wide range	Sphere with equivalent sedimentation time	Moderate
SAXS		Wide range	Detects primary particles	High
DLS		Wide range	Does not resolve agglomerates	High
HCPCF		Very concentrated	Particle with equivalent optical signal	Minimal
spICPMS	Particle by particle	Very dilute	Particle with equivalent mass	Minimal
NTA		Very dilute	Sphere with equivalent diffusion coefficient	Minimal
TRPS		Very dilute	Sphere with equivalent volume	Minimal
DMA-CPC		Very concentrated	Sphere with equivalent aerodynamic mobility	Minimal

We evaluated the performance of five laboratory methods by using a set of four samples made of 80 nm gold nanoparticles with different agglomeration states. This was induced by functionalising the particles with PEG-biotin and introducing different amounts of Avidin in the samples, see Table 9. Generating samples with consistent aggregation states that were stable over time and after dilution was a significant challenge. The samples analysed here represent the culmination of a significant effort.

**Table 9.** Sample description and concentration of primary particles as measured by UV-Vis spectroscopy.

Sample name	Monodispersed nanoparticles	Agglomerated nanopartilces	[C] <sub>NCAvd</sub>	UV-Vis [C] (10 <sup>9</sup> Particles mL <sup>-1</sup> )
Agg1	100%	-	-	7.1
Agg2	67%	33%	0.14 µM	6.8
Agg3	33%	67%	0.29 µM	6.4
Agg4	-	100%	0.44 µM	6.0

UV-Vis spectroscopy was used to measure the total number of primary particles in the samples, which is reported in Table 9. These values were measured as described in section 4.1.3 with similar measurement uncertainty of about 20 %. The measurement results are summarised in Figure 4. Among all the laboratory methods, DCS, NTA and to some extent spICPMS were able to discriminate particle populations with different level of agglomeration. On the contrary, DLS did not have sufficient size resolution to discriminate the agglomerates. DCS was the only method that could provide a detailed description of the state of agglomeration of the samples. If this information is of significant importance, then DCS should be made one of the methods of choice for the measurement of particle concentration. However, our comparison study clearly shows that

while DCS can provide quantitative information of the *relative* concentration of particle populations in a sample, it systematically underestimates their absolute concentration (see section 4.1.5).

Within this project we developed an accurate approach to measuring *absolute* particle concentration for agglomerated gold nanoparticles. By calibrating the DCS relative concentrations with total gold concentrations from UV-Vis spectroscopy we obtain accurate measurements of absolute and relative particle concentrations [paper 9]. This is an outstanding result, enabling the calculation of both number and mass concentrations in the total population and individual sub-populations of aggregated samples as well as the calculation of variously weighted (e.g. by number or mass) average particle sizes. SAXS was also considered for accurate measurements of aggregation state, using the Guinier region intensities. However, the sensitivity of the method was insufficient and no simple model to describe this region could be developed within the consortium.

Although the size resolution of PTA and spICPMS is inferior to DCS, the absolute number concentration measured by these methods is more accurate. The value for Agg1, the monodisperse sample, is within 7% of that measured by UV-Vis spectroscopy. As far as the number concentrations of particles is concerned, the two techniques are within 14 % and both techniques are within 10 % agreement with the concentrations measured by using a combination of DCS and UV-Vis spectroscopy. This level of agreement is within the uncertainty of the accurate value and we therefore conclude that the DCS+UV-Vis, PTA and spICPMS can be accurate for measuring the concentrations of aggregated gold particles. DCS on its own is inaccurate, by a factor of two in this case but this is consistent with the general inaccuracy of the method. DLS is also inaccurate by a factor of three here.

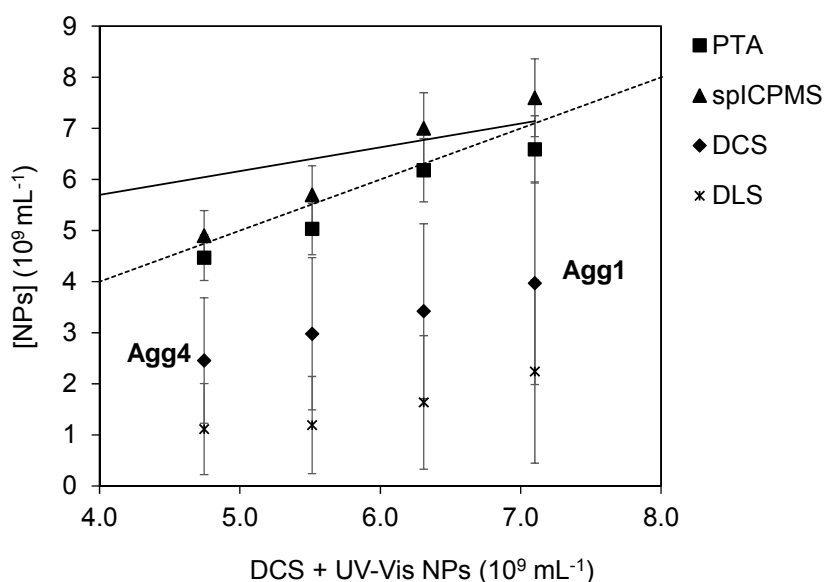


**Figure 4.** Comparison of laboratory methods for the measurement of concentration of monodisperse (Agg1) and agglomerated (Agg2, Agg3, Agg4) gold nanoparticles. Particle concentration is shown as a function of those accurately measured through calibrated DCS. The dashed line represents equality with the accurate value, the solid line represents the number concentration of *primary* particles directly from UV-vis.

The results do not include data from SAXS, TRPS, HC-PCF and ES-DMA-CPC. These methods were investigated during the project, but significant experimental challenges made it impossible to acquire meaningful data for the comparison of concentration measurements. SAXS was not able to detect agglomerated particles and only measured the total concentration of primary particles. This information was already provided with accuracy by UV-Vis spectroscopy, which was selected as a method of choice given its accessibility and easiness of interpretation. The conditions required for TRPS measurement resulted in further aggregation of samples. Both HC-PCF and ES-DMA-CPC were insufficiently sensitive to measure these samples.

#### 4.1.8 Conclusions

Accurate measurements of the concentration of colloidal nanoparticles, spICPMS and SAXS, were developed and demonstrated using gold, polystyrene and silica nanoparticles. For gold particles, excellent agreement was obtained between the accurate methods to within their ~10% uncertainties. UV-vis spectroscopy was also

shown to be accurate for gold particles in water. Only SAXS was applicable to polystyrene and silica particles and in both cases there were significant discrepancies with laboratory based methods, some of which were explicable on the basis of uncertainties in refractive indexes and densities. A series of mixed samples highlighted which methods were capable of measuring absolute and relative number concentrations of mixed nanoparticle populations, in this regard PTA provided the best accuracy for the particle populations which could be detected. DCS also provided consistent results and was able to detect a larger range of particles.

Accurate methods were established for analysing aggregated and non-spherical gold particles using a combination of UV-vis spectroscopy and DCS. The performance of a range of laboratory methods were evaluate for the measurement of the number concentration of agglomerated particles. Comparable results were obtained from five methods, namely PTA, spICPMS, DCS, DLS and a combination of DCS and UV-Vis spectroscopy. With the exclusion of DLS (which is not designed to measure particle concentration) and DCS, the remaining three techniques showed to be in agreement within 14%, which is a value comparable with their measurement uncertainty.

## Traceable Measurement of Shell Composition and Thickness

*This Chapter addresses Objective 3*

### 4.2.1 Introduction

The aim of this work was to establish traceable chemical methods for the amount of substance in a nanoparticle coating. The behaviour, performance and fate of nanoparticles is inextricably linked with their surface properties. For example, for most particles colloidal stability depends upon the existence of an electrical charge on the particles. If all particles have the same charge then they repel each other and, provided that this electrical interaction overcomes Brownian motion, the particles do not stick together. The charge is determined by the chemical groups on the surface of the particle. In other instances, such as quantum dots, the particles require a coating to prevent the environment interfering with the properties of the core material. In biomedical applications, coatings prevent the adhesion of biological molecules, or provide selective binding of one type of molecule. To determine the amount of substance it is necessary to have analytical techniques that provide both the chemical identity of the coating and its thickness. Additionally, for a number of biological and chemical applications it is important to understand the accessibility of reactive sites, such as functional groups, in the coating.

A number of techniques are available which can assess the thickness of the shell on a nanoparticle, a few of which are also able to provide a measure of the elemental or chemical composition of the shell material. **Table 10** lists the techniques considered within the project and some of the restrictions that apply to them. It is also possible to measure the average amount of material in the shell through the measurement of particle size and an assumed core size. Methods such as DLS, DCS, TRPS described in section 4.1 are capable of this and this was performed on some of the samples as part of the project as additional validation. We note that these methods require either additional data or an assumption. For example, in the case of a single measurement the size of the core must be known. These techniques are not listed in the table, which includes only those that are capable of a direct measurement of shell thickness and chemistry.

**Table 10:** Techniques capable of measuring the physical thickness of a shell. The term “robust” signifies that the particles should be made of materials which do not damage during electron beam irradiation.

Technique	Chemistry	Measured quantities	Comments
SAXS	N	Angular dependent scattered X-ray intensity	Restricted to monodisperse spherical particles. Requires core-shell density contrast and modelling.
TEM	N	Electron transmission or scattering	Restricted to isolated, dry, robust particles. Requires significant core-shell contrast.
ISS	Y	Energy and intensity of scattered ions	Restricted to dry particles. Requires detailed modelling.

XPS	Y	Electron energy and intensity	Restricted to dry particles. Requires detailed modelling.
AES	Y	Electron energy and intensity	Restricted to dry, robust particles. Requires detailed modelling.
XSW / XRS	Y	X-ray intensity	Restricted to monolayers of monodisperse particles. Requires specialised equipment and expertise.

Of the methods listed, the majority require the particles to be in the dry state. The exception is SAXS which can be employed directly on core-shell particles in suspension. Because the focus of the project is on the analysis of colloidal suspensions of nanoparticles, it is important to recognise that the preparation required to take the particles from liquid suspension and dry them for analysis can introduce artefacts and errors.

#### 4.2.2 Samples

##### *Core-Shell Particles*

A range of different core-shell particles were useful and these are outlined in **Table 11**. Many of these were imaged by electron microscopy to obtain estimates of core and shell thickness.

**Table 11:** List of core:shell particles studied in the project

Core	Shell	Supplier	Nominal [Core D: Shell T] (nm)	Comments
Gold	Organic	NPL	[60: 3], [30, 100, 250: 2]	Uniform shell thickness
PTFE	PMMA	UPO	[47: 5, 12, 24, 35]	Polydisperse core
PTFE	PS	UPO	[47: 6, 10, 17, 24, 34, 48]	Incomplete shell
Pt	TiO <sub>2</sub>	BHAM	[1.4: 0.9]	Low production rates

##### *Organic coated gold particles*

Citrate stabilised gold particles from BBI Solutions (Cardiff, UK) were incubated with a peptide (sequence CGGGNPSSLFRYLPSD) obtained from GenScript (Piscataway, USA) in buffer for 1 hour. The peptide contains a reactive thiol group in the terminal cysteine group which binds to gold to form a uniform coating. On flat gold surfaces this peptide had previously been shown to form a uniform layer of approximately 3 nm thickness on gold nanoparticles over a large range of core diameters. A set of PEG-functionalised gold nanoparticles were with size ranging from 30 nm to 250 nm were produced and analysed by DCS and DLS. Thermogravimetric analysis was attempted but did not provide accurate results due to the relatively small amount of gold contained in the samples.

##### *Polymer particles*

The PTFE-PMMA and PTFE-PS core-shell nanoparticles were synthesized by emulsifier-free batch seeded emulsion polymerization in the presence of PTFE seed particles. The employed PTFE suspension (Hyflon MFA 100 LS latex) was kindly supplied by Solvay Specialty Polymers and it is a special grade of a perfluoroalkoxy polymers resulting from the polymerization of tetrafluoroethylene (TFE) and perfluoromethylvinyl ether (PFPME). Particle total diameters were measured by SEM, nominal thicknesses were calculated from the difference between the SEM diameter and that of the PTFE cores after relevant adjustments for the estimated thickness of the conductive coating required for SEM analysis. Analysis by TGA confirmed that the mass ratio of shell material to PTFE core was consistent with the feed ratio of monomers to core particles. Furthermore, DCS analysis confirmed that an average core size of 47 nm was consistent with the sedimentation rates, but suggested that the density of core was significantly (~25 %) lower than that of crystalline PTFE.

##### *Platinum in titania particles*

The nanoparticles were produced through gas condensation using a magnetron sputtering cluster source with base pressure of 10<sup>-7</sup> mbar. An alloy target of Pt-Ti alloy was used with Pt to Ti mass ratio of 25 % to 75 %

(Target purity 99.95%), corresponding to 13 Ti atoms for every Pt atom. The magnetron was used in DC mode. Argon gas was used to create the plasma for sputtering. In addition, Helium gas was injected into the chamber to promote aggregation. Liquid nitrogen was used to cool down the gas mixture to further enhance aggregation. The nanoparticles were mass selected using a lateral time-of-flight mass selector with resolving power  $M/\Delta M = 20$ . The nanoparticles were soft-landed on either: copper TEM grids covered with amorphous carbon films for electron microscopy or silicon wafers for surface chemical analysis. Particles with average size 30000 Da formed a core-shell structure with Pt core and  $\text{TiO}_2$  Shell. Scanning Transmission Electron Microscope (STEM) in High Angle Annular Dark Field (HAADF) Mode was used to investigate the Monodispersity and storage time of the particles. The samples were analysed on a period of 6 months and the particles demonstrated to be stable over the period. The core size was measured to be  $1.4 \pm 0.2$  nm with a shell thickness of  $0.9 \pm 0.3$  nm as shown in **Figure 5**.

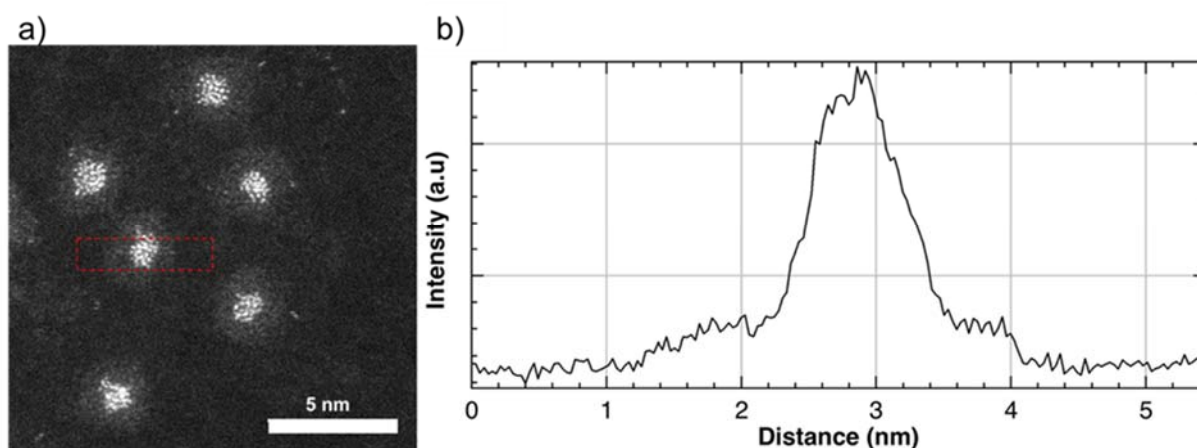


**Figure 5:** (a) HAADF STEM image of the 30000 amu core-shell nanoparticles. The bright cores in the middle are Pt and the halos around these cores are  $\text{TiO}_2$  (b) Averaged line profile of the dotted red rectangle on the nanoparticle.

#### 4.2.3 SAXS and XSW Analysis

These synchrotron-based methods were employed to confirm the core-shell structure of some of the materials investigated in the project.

##### SAXS Analysis

The SAXS analysis should, in principle, be able to determine accurate measurements of core diameter and shell thickness. However, this is practically possible only on materials with highly defined characteristics: low dispersity in core diameter, low dispersity in shell thickness, ideally spherical and centred cores. Such well-defined characteristics were only approached for the gold:organic particles but unfortunately the density contrast between gold and organic material is very large and the contrast between the organic shell and water very small these factors make meaningful SAXS measurements impossible. In a practical context, it became clear that such well-defined systems were not available and therefore of little practical value in an industrial context. Therefore, the work focussed upon the metrological needs of industry in terms of how to extract a useful mean value of shell thickness, measure the average chemical compositions of the particles and how to identify and account for less than perfect core:shell particles.

In order to analyse the SAXS data a special acentric core-shell form factor was developed with an additional routine to fit several curves for different electron density contrasts at once. However, this could only be applied to the HM series because the particles from PTFE:PS series showed a non-spherical shape as well as an extremely displaced core and the shell of PS gives naturally a very low scattering contrast. Example scattering curves obtained by the fitting procedure are shown in **Figure 6** for PTFE cores and the PTFE:PMMA [27:35] samples. From these curves the size and structure of the nanoparticles can be estimated.

The fit of the cores with log-normal distribution shown for the PTFE cores gave a diameter  $31.2 \pm 4.1$  nm with a significant polydispersity. The results of the fits for the full range of PTFE:PMMA particles provided core diameters between  $25 \pm 4$  nm to  $28.8 \pm 4.2$  nm for the [47:5] sample. The difference to the naked cores could lay in the polydispersity of the cores (different average size) or in the nature of the model, which assumes a

strict density border between core and shell. The fact that the core diameter is closest to the value of the naked cores for the sample with lowest shell thickness supports the second explanation.

The total diameter of these PTFE:PMMA particles was typically closer to those observed by DLS, in contrast to those observed by SEM. As SAXS measures the physical particle diameter rather than the hydrodynamic diameter, and is insensitive to particle agglomeration, it is expected to give slightly smaller diameters than the DLS, particularly for the larger particles where a greater degree of agglomeration is expected. The larger diameters when compared to SEM measurements is most likely due to other effects, such as electron beam damage of the particles in SEM, and possible swelling of the polymers in solution.

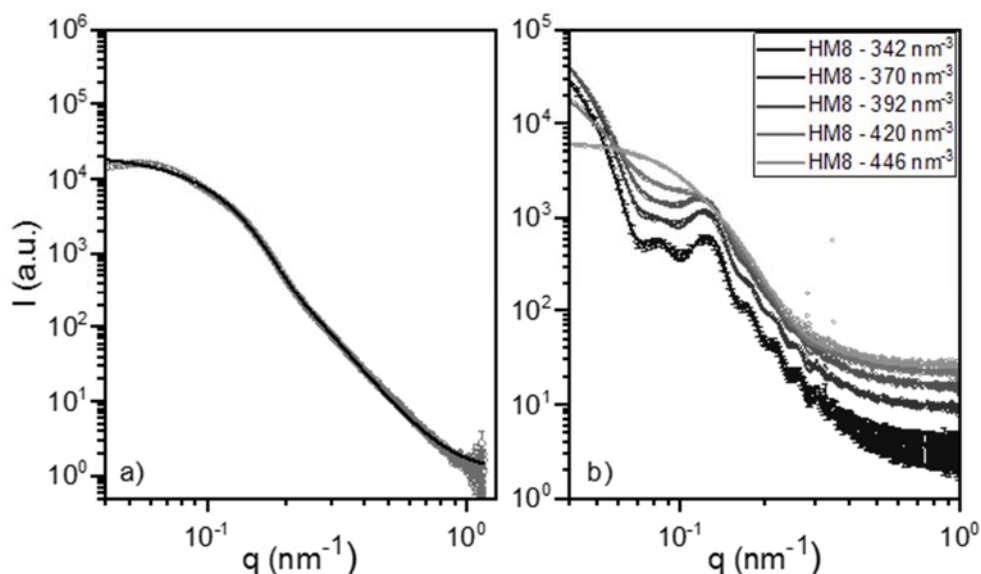


**Figure 6:** Scattered intensity obtained by SAXS (a) Naked PTFE cores fitted with lognormal size distribution (b) sample PTFE:PMMA [47:35] for different solvent electron densities and according fits. The curves have been offset vertically for better visibility.

#### XRF Analysis

Pt-Ti core-shell nanoparticles were used to investigate the modification of the XSW field intensity with increasing surface coverage. Therefore, reference-free GIXRF methods were also used for the quantification of the core-shell nanoparticle elemental composition and surface coverage. In order to link dimensional with analytical nano-metrology, the areal weight ratio of titanium and platinum must be known. The areal weight ratio is the ratio of the mass deposition between Ti and Pt. The elemental composition of the core-shell nanoparticles is analysed using reference-free GIXRF. The excitation energy was set to 12.5 keV, which is above the titanium K- and the platinum L3 edges. The incident angle was set to  $0.125^\circ$  with respect to the sample surface, which is below the critical angle of total external reflection, in order to have a decent signal-to-background ratio. The quantification with reference-free XRF of both elements leads to a Ti:Pt areal weight (mass) ratio of 0.63(5) : 0.37(5) as against the nominal 0.75 : 0.25 sputter target ratio. The information on the mass ratio is independent of the absolute mass deposition, which is why an even simpler approach can be used for the determination of the surface coverage. The instrumental and experimental parameters such as the solid angle of detection and the incident photon flux are the same for both quantifications and therefore do not contribute to the uncertainty budget in this case. The main contributions to the uncertainty budget are the relevant fundamental parameters. Furthermore, the total mass of the elements deposited onto the surface could be determined and from this, the surface coverage calculated. This was found to be in reasonable accord with the nominal coverage estimated from TEM measurements and the duration of the deposition of particles, one of the factors that contributed to the difference was a lateral inhomogeneity in the amount of nanoparticles deposited.

#### XSW Analysis

The surface coverage of the Pt-Ti core-shell nanoparticles also influences the intensity distribution within the XSW field. For a very low surface coverage, the XSW field above the surface of the reflecting medium is undisturbed, and can in the present case, be calculated using the optical constants of the silicon substrate and vacuum above the reflecting surface. With increasing coverage, the reflection properties of the surface change

due to the nanoparticles and have to be taken into account in the XSW field calculation. Using an effective density approach, where the nanoparticles are assumed to be a continuous layer with reduced density to take into account the coverage, this can be done. Such calculations, which were performed using software developed in-house are shown in **Figure 7** (left-hand side) in comparison with the experimental Ti-L fluorescence GIXRF measurements. Here, for the samples with nominal 2.5 %, 5.0 %, 30 % and 60 % surface coverage, the relative intensity of the peak at the critical angle of total external reflection is clearly decreasing with increasing coverage, whereas the angular position of the peak does not change significantly. The same behaviour is found for the calculated curves, assuming a thin layer with varying density. This clearly demonstrates that the particles must be taken into account during the XSW field calculation.

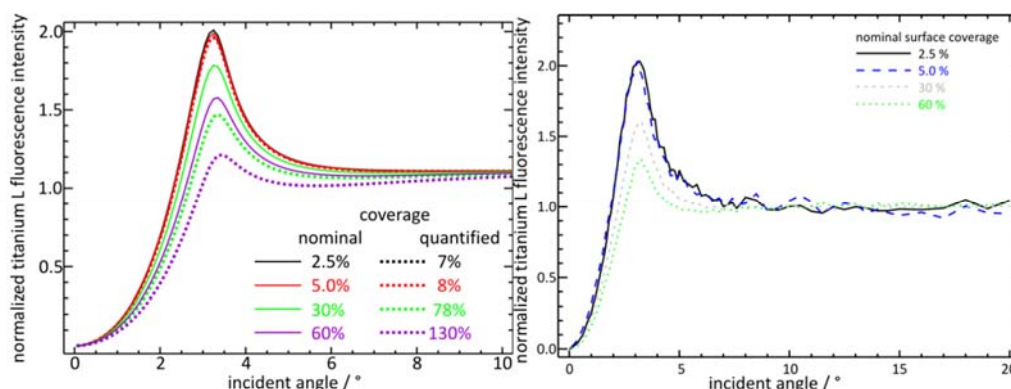


**Figure 7:** Calculated relative XSW field intensity (left) and GIXRF measurements in the soft X-ray range (titanium L fluorescence lines) of all samples with different nominal surface coverage (right). The shape of the curve indicates different intensities of the XSW field. At high incident angles, the excitation radiation is penetrating into the sample and is not reflected anymore, so that no relevant XSW contribution occurs.

#### 4.2.4 Electron Spectroscopies

##### *Sample preparation*

As soon as it comes to investigation of nanoparticles with XPS, sophisticated sample preparation is crucial, in order to ensure reliability and reproducibility of the results. It should be stressed at this point that, due to the broad variety of material-morphology combinations, a generally applicable sample preparation routine for core-shell nanoparticles has not been identified, but useful protocols for specific samples were. Such a routine must always be tailored to the specific combination of nanoparticle, solvent and substrate. The procedures that were developed by the three project partners BAM, NPL and TUW to deposit the PTFE-PMMA core-shell nanoparticles on a silicon wafer surface. The understanding developed in the project was incorporated into an international standard which was developed during the project and led by a project collaborator, Pacific Northwestern National Laboratory, USA: ISO 20579-4 "Surface Chemical Analysis - Sample handling, preparation and mounting - Part 4 – Reporting information related to the history, preparation, handling and mounting of nano-objects prior to surface analysis".

An example procedure is provided below in **Table 12**. In the case of insulating nanoparticles, such as the model nanoparticle investigated here, the preparation is particularly challenging. A compromise must be found between a particle layer that is, on the one hand, thick enough to prevent the substrate from significantly contributing to the spectrum and, on the other hand, thin enough to avoid differential charging effects. Such effects can be shifting and broadening of peaks leading to severe distortion of spectra. They originate from insufficient compensation of positive charge left after photoionization. This especially applies to measurements at XPS spectrometers where no charge compensation is available. However, all partners responsible for this work used instruments enabling active charge compensation. In the case of conductive nanoparticles, it is equally important to generate a closed, uniform particle layer, however, it can be rather thick without facing any problems with charging effects. Therefore, drop-casting is the deposition method of choice for producing reliable and reproducible XPS spectra. A clear advantage of the drop-casting deposition technique is its simplicity, a clear disadvantage its inefficiency in terms of time.

**Table 12.** Recommended procedure (SOP) for preparation of insulating core-shell nanoparticles for XPS experiments (in polar solvent)

#### Preparation of nanoparticle suspension with suitable concentration

- diluting of initial suspension
- concentrating of initial suspension (zentrifugation or evaporation of solvent)

#### Increasing the hydrophilicity of the substrate

- plasma treatment
- UV/ozone treatment

#### Application of single drop of suspension onto the substrate

- when sample is already in spin-casting instrument
- just before rotation starts, since drop must not dry before rotation

#### Spin-casting

- phase 1: slow speed (~5s), phase 2: higher speed (~20s)
- speed high enough to thoroughly distribute the particles
- speed not high enough to spin all particles off the substrate

#### *Validity and accuracy of XPS*

The estimation of shell thicknesses of CSNP is influenced by a considerable number of uncertainty sources that will be discussed briefly. These sources can be divided into three categories, those that are related to the model calculations, those originating from the experimental procedure (preparation and handling of samples as well as the XPS measurements) and irregularities in the CSNP geometry that deviate from the assumption of perfectly spherical and concentric CSNPs.

#### Uncertainty sources of the model calculations

The most crucial parameters for the calculation of shell thicknesses are the inelastic mean free paths (IMFPs) of the different photoelectron species in the core and shell materials. For the model calculations, all IMFP values were calculated using the TPP-2M (Tanuma – Powell – Penn '2M') formula which is typically assumed to exhibit uncertainties of the order of 10 %. In the model calculations, predicted signal intensities and shell thicknesses are expressed in units of the IMFPs. Therefore, the uncertainty of the IMFPs dominate the uncertainty budget of the shell thickness estimations and can be regarded as a lower boundary for the shell thickness uncertainties.

Proportionality factors such as the photoionisation cross sections (PCSs) and relative sensitivity factors (RSFs) that depend on the PCSs are commonly assumed to exhibit uncertainties of the order of 10 % as well. However, a change in the intensity ratios by 10 % only leads to a change of about 2 to 3 % in the retrieved shell thickness. In the most thorough studies, as in the case here, experimental peak intensities are used from reference materials and this reduces the error further.

Since the core size is an input parameter of shell thickness estimations, a dispersity in the core radii is a source of uncertainty. However, differences in the exact core radius value only have a very small influence on the shell thickness result if the core radius of a CSNP larger than the IMFPs in the core material, as is the case for most samples. Furthermore, if the distribution of core radii is roughly symmetric, positive and negative deviations cancel out each other. Therefore in the present case, it is a very good approximation to neglect the core size dispersion and only regard the mean core radius for all calculations.

Elastic scattering is neglected in the approximate models tested in this work. Neglecting elastic scattering is commonly referred to as the straight line approximation (SLA). SESSA simulations were performed with and without the SLA, allowing a direct estimation of the significance of elastic scattering. The influence of elastic scattering on shell thickness estimation strongly depends on the shell material and it was shown that in the

case of organic materials the SLA is an excellent approximation. As expected, the SESSA simulations with elastic scattering yield slightly lower shell thicknesses than the calculations employing the SLA with deviations of less than 10 %. For each type of CSNP it should be decided on a case-by-case basis whether elastic scattering can be neglected or not. However a reasonable adjustment can be made by using the Effective Attenuation Length (EAL) of the electrons in the material in place of the IMFP. A series of papers by consortium partners in collaboration with Cedric Powell from NIST has confirmed that this is a valid approach.

#### Sources of uncertainty in the experimental procedure

It is known that nanoparticles are susceptible to changes over time and induced by various external influences, including storage temperature, oxidation due to air exposure, vacuum stability and radiation damage during the XPS measurements. Depending on the stability of the investigated nanoparticles the exact experimental procedure may change the shell thickness results. Most importantly, the sample preparation procedure can have a drastic influence on the condition of the nanoparticles at the time of the XPS measurement. While the PTFE:PMMA particles are regarded as relatively stable, the differences in the partners' experimental procedures are assumed to be the largest contribution factor to the deviations observed in the comparison within this project. Nevertheless, the observed consistency between the partners' results is very satisfying. A VAMAS study inter-lab study with a larger number of participants [Paper 3] completed as part of this project showed far larger deviations between individual results on samples prepared by some participants.

The determined signal intensities depend on the background subtraction and the peak fit. In the present case, the ionisation edge heights were relatively small with respect to the peak heights and the peak fits benefitted from well separated peaks. The uncertainties of the determined signal intensities were therefore regarded as less critical, but a case-by-case consideration is necessary. Uncertainties of this nature can be regarded similarly to PCS uncertainties (see above).

Irregularities and non-ideal geometries of the particle includes non-uniform shell thicknesses in single particles, a disperse shell thickness distribution across the entire sample, acentric core positions and porous or incomplete shells. All of these constitute deviations from the idealised model on which all model calculations were based and have been observed by other experimental techniques such as TEM and SAXS. To some extent, statistical distributions of these irregularities are expected to lead to cancelling and a mean shell thickness results from the calculation. However, careful analysis shows that XPS will always underestimate coating thickness if there is a variation in thickness across a sample. This is illustrated in **Figure 8** in which the fluorine signal from the PTFE is plotted as a function of average shell thickness.

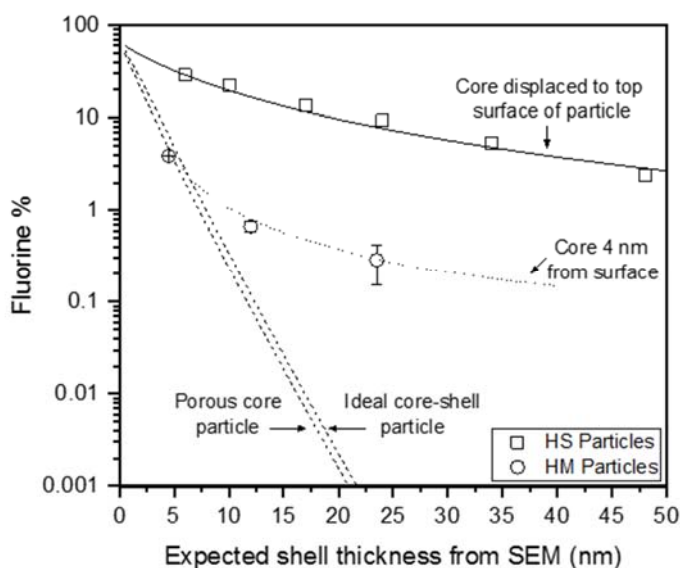


**Figure 8.** Calculated fluorine intensity in XPS expressed as equivalent atomic % for various core-shell structures. HS data points are the PTFE:PS particles which have an exposed core. HM data points are PTFE:PMMA particles in which the data are consistent with an off-centre core.

Since the calculation of IMFPs is regarded as the dominating uncertainty source of shell thickness estimations, an in-depth study of optical constants and IMFPs of organic materials (including PMMA and PTFE) was

conducted. Generally a good agreement with the TPP-2M formula [8] was found with the exception of PTFE which showed a drastic deviation between the determined IMFP and the TPP-2M formula prediction. A peer-reviewed publication is currently in preparation.

#### Laboratory XPS

A specific model nanoparticle consisting of a polytetrafluoroethylene (PTFE) core surrounded by a poly(methyl methacrylate) (PMMA) shell was prepared within the consortium. The particles were carefully pre-characterised by SEM to determine core diameter and shell thickness. The particle was measured by laboratory XPS and the results, including information about sample preparation procedure, XPS acquisition parameters and data evaluation were analysed for the purpose of mutual validation. Furthermore, four different algorithms for the determination of shell thicknesses from XPS intensities were compared by different partners within the consortium: SESSA accounting for elastic scattering effects, SESSA using the SLA, the IC model and the  $T_{NP}$  model.

The chemical compositions independently determined by three project partners are in very good agreement. The standard deviation of the carbon contents is 0.7 %, of the oxygen contents 3.6 % and of the fluorine contents 12.8 %. The first two deviations are well within the targeted uncertainty of 10 %, while the third is slightly higher which could be explained by x-ray beam damage to the PTFE.

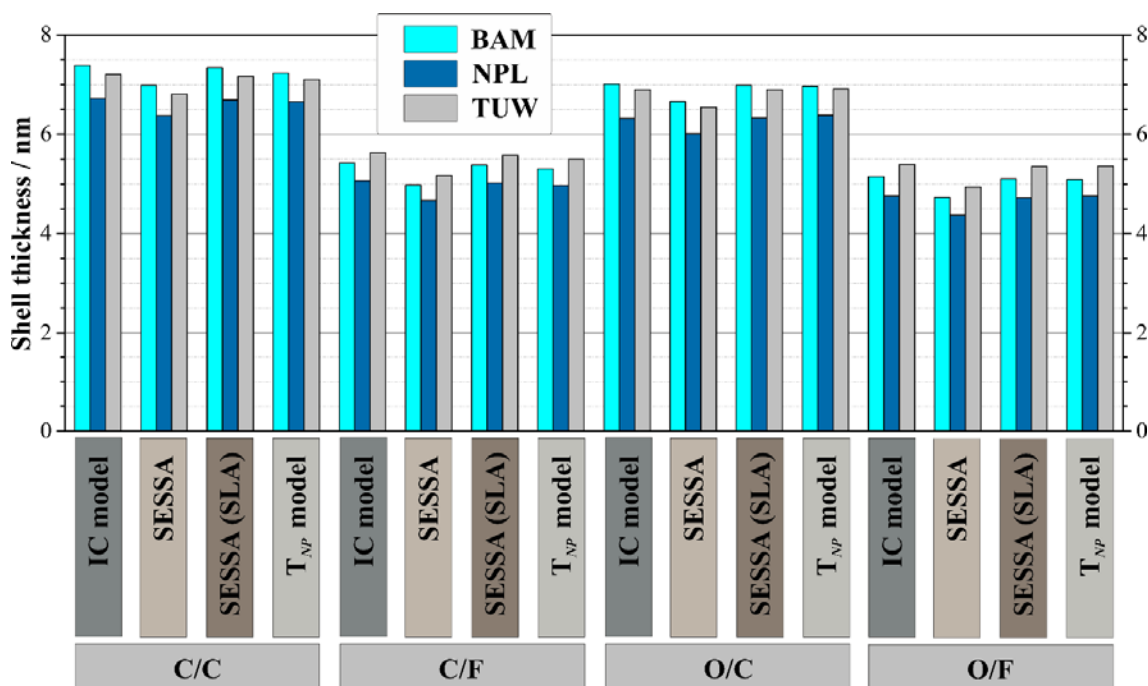


**Figure 9:** Thicknesses determined by IC model, SESSA with elastic scattering, SESSA without elastic scattering and  $T_{NP}$  model. The plot contains the results for all shell/core element intensity ratios of the three project partners.

**Figure 9** shows the shell thicknesses derived from all four theoretical models, from four different shell/core XPS intensity ratios and from three project partners. There is a very good agreement (below 10 %) of the shell thicknesses calculated from the XPS intensities when comparing the values from different theoretical models from the same intensity ratio and the same project partner. Also the comparison of shell thicknesses calculated from the datasets of different institutions for the same intensity ratio and the same theoretical model reveals a good agreement (approx. 10 %). When comparing the results obtained from the different datasets provided by the three partners, the corresponding shell thickness deviations are in the order of 10 %. This deviation is likely due to a combination of different sample preparation, peak fitting procedures, and transmission function corrections. While still significant, the deviation is considerably less than previously reported interlaboratory deviations in nanoparticle shell thickness measurement. The largest deviations are observed when comparing the shell thickness estimates resulting from the intensity ratios of the four different line pairs. The reason could be some more significant structural or compositional defect. However, a final conclusion is not possible based on the available data and would require a more detailed investigation such as be energy-resolved XPS experiments.

These results show that the determination of chemistry and shell thickness to a target uncertainty of 10 % is challenging, but possible. It becomes clear how crucial it is for shell thickness determination from XPS intensities to have reliable, accurate reference measurements e.g. from electron microscopy.

### Synchrotron-XPS

The nanoparticles investigated by synchrotron-XPS were strontium fluoride ( $\text{SrF}_2$ ) cores surrounded by a calcium fluoride ( $\text{CaF}_2$ ) shell synthesised by the project stakeholder Nanofluor GmbH (Berlin, Germany). The nanoparticles were pre-characterised by TEM and DLS. A suitable sample preparation method for this specific nanoparticle system had to be found that would ensure an acceptable quality of the synchrotron XPS spectra. A compromise had to be found between a particle layer that is, on the one hand, thick enough to prevent the substrate from significantly contributing to the spectrum and, on the other hand, thin enough to avoid charging effects such as shifting of peaks, broadening of peaks or even the appearance of new false signals. This task was even more challenging due to the low performance of the charge compensation device at the XPS spectrometer that was used. In the end, a combination of particle purification, UV/Ozone cleaning of the substrate and drop-casting of a relatively diluted suspension was identified as the optimum procedure.

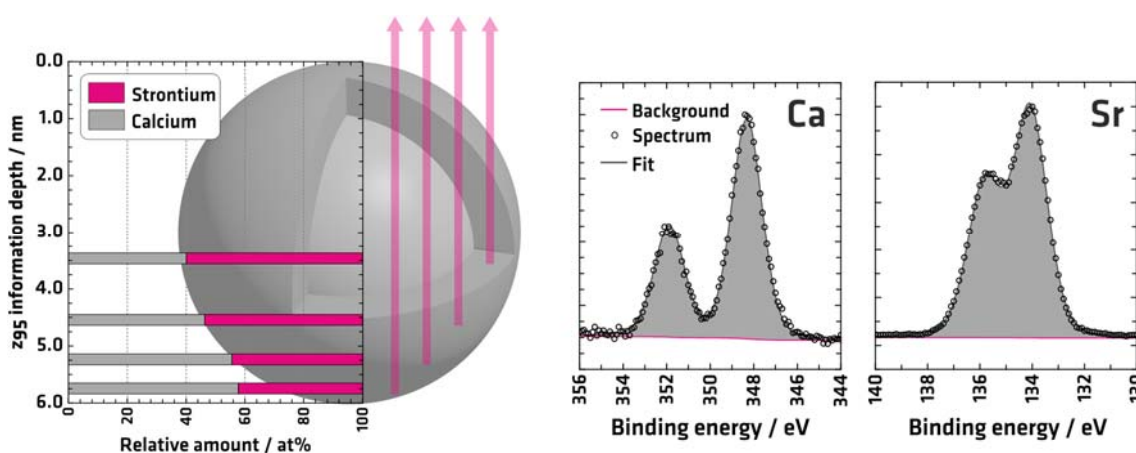


**Figure 10:** Depth profile from synchrotron-XPS experiment combined with a graphical representation of the information depth relative to the particle size (left). Spectra containing Ca2p and Sr3d doublets at an excitation energy of 525 eV (right).

The variable x-ray energies available at the synchrotron facilitate a variation of the XPS  $z_{95}$  information depth. The  $z_{95}$  information depth is defined as three times the IMFP of the photoelectrons through the shell material  $\text{CaF}_2$ . In order to generate such a depth profile for the  $\text{SrF}_2$ - $\text{CaF}_2$  core-shell nanoparticles, high-resolution spectra of the Ca2p and Sr3d signals were recorded at 849, 775, 676 and 525 eV X-ray excitation energy. Since it is the intention to more accurately characterise the core-shell structure of the nanoparticles, one signal from the core and one signal from the shell was selected.

The relative amounts of calcium and strontium in the sample are plotted in **Figure 10** as a function of the  $z_{95}$  information depth. With increasing  $z_{95}$  information depth the calcium/strontium ratio is also increasing. These results have to be treated as preliminary results, as a reliable transmission function for the respective XPS spectrometer could not yet be determined. However, the values seem reasonable assuming that a single nanoparticle and the XPS information depth are of the same order of magnitude.

### AES

Two different types of core shell nanoparticles were investigated using Auger electron spectroscopy (AES): Firstly, gold (Au) nanoparticles with a silver (Ag) shell purchased from nanoComposix (San Diego, USA) and, secondly, sodium yttrium tetra-fluoride ( $\text{NaYF}_4$ ) nanoparticles with a silica ( $\text{SiO}_2$ ) shell synthesized by division 1.2 of BAM (Berlin, Germany). The particle core is doped with 2 % europium (Er) and 20 % ytterbium (Yb) ions. In the case of the Au-Ag core-shell nanoparticles, two different samples with different core diameter and shell thickness were examined. All samples were pre-characterized by TEM. Even after the purification of the Au:Ag core:shell particles a signal from the gold core could not be detected in the AES spectra, but only from the silver shell. Furthermore, the analysis of single particles using line scans and SAM mapping yielded total particle diameters in very good agreement with TEM. In the case of the  $\text{NaYF}_4$ : $\text{SiO}_2$  particles, after purification of the samples the elements F and Y from the particle core could be detected in the AES spectra next to Si from the shell material. Line scans of single particles were recorded reflecting size and position of the particle core relative to the particle centre.

### STXM

A STXM based methodology was developed for determining the dimensions (shell thickness, core and total diameter) of core-shell nanoparticles. A corresponding paper has been published with open access in Surface and Interface Analysis [**Paper 5**].

### NAP-XPS

Two systems of suspended nanoparticles have been studied with NAP-XPS: Ag nanoparticles in water and SrF<sub>2</sub>:CaF<sub>2</sub> core:shell nanoparticles in ethylene glycol. Shell-thicknesses of the latter nanoparticles were estimated based on simulated spectra from the software SESSA. A corresponding paper has been published with in the Journal of Physics: Condensed Matter [**Paper 4**].

### 4.2.5 Surface Measurements from Colloidal Particles

The aim of this work was to investigate easy and robust methods that may be used by industry to determine the surface chemistry of particles in colloidal suspension. These methods include electrophoretic mobility ('zeta potential') measurements and tunable resistive pulse sensing (TRPS), second-harmonic generation (SHG) and Raman spectroscopy in hollow-core fibers, as well as conductometric titration and dye-based optical assays with photometric or fluorimetric detection. Whereas zeta potential measurements, TRPS, SHG, Raman, and conductometric titration may reveal the total concentration of (deprotonable/protonable) functional groups, labeling-based assays that apply photometric or fluorimetric detectable dyes yield the amount of functional groups that are accessible for further (bio)functionalization.

#### *Tunable Resistive Pulse Sensing (TRPS):*

This method is described in 4.1.4. The electrophoretic mobility of the particle can be determined from the duration of the blockade event. Effects such as electro-osmosis and pressure differences need to be taken into account, and calibrant particles with a known zeta potential are required. Data was analysed using the software provided by the manufacturer (Izon Science Ltd.).

#### *Hollow Core – Photonic Crystal Fibre (HC-PCF):*

This method is described in 4.1.4. The particles are analysed through light scattering processes which result in the generation of different wavelengths to the incident light. SHG, the generation of light of twice the incident frequency has been reported to be sensitive to surface charge on particles. Proof of principle experiments demonstrated the generation of SHG from gold nanoparticles, but within the HC-PCF the gold particles could not be detected, see section 4.1.4.

#### *Conductometric titration:*

Electrochemical titration methods utilize the smallest possible reporters (H<sup>+</sup> and OH<sup>-</sup>) for signal generation and thus yield the maximum number of accessible functional groups (FG), which typically equals the total number of (de)protonable surface functionalities. Conductometric titration is inexpensive, but requires a relatively large amount of sample and prolonged equilibration times, and is sensitive to ionic contaminations (e.g. initiators from radical polymerization reactions, stabilizers, and salts). FG quantification via conductometric titration was performed using HCl titer (titration) and NaOH titer (back titration), at which the order of titration does not matter. For complete protonation or deprotonation of the FG on the NP surface prior to the titration, the conductivity of the suspensions was adjusted to 100 μS/cm with HCl or NaOH, respectively. Titration is then separated into three segments: neutralization of excess H<sup>+</sup>/OH<sup>-</sup>, (de)protonation of FG on the NP, and increasing excess of H<sup>+</sup>/OH<sup>-</sup>. Subsequently, back titration consists of the same processes in reversed order. The different segments are determined by the intersection points of the fitted linear functions, and the applied volumes between the equivalence points are proportional to the number of (de)protonatable groups.

#### *Dye labeling-based optical assays:*

Optical methods like spectrophotometry and fluorometry require an absorptive or emissive label (e.g. an organic dye) covalently attached or adsorbed to the FG on the NP. As dye reporters have a larger size compared to H<sup>+</sup> and OH<sup>-</sup>, these assays typically yield a smaller amount of FG with respective stoichiometry factor depending on label size, which provides information on the mean number or density of accessible (derivatizable) FG required for subsequent NP (bio)conjugation reactions. Dye-based optical assays involve the labeling with (i) conventional dyes such as NHS-fluorescein (for NH<sub>2</sub> groups) or 6-amino fluorescein (for COOH groups after activation with EDC/NHS or HATU) with spectral features that are not affected by conjugation; (ii) dyes that change their spectroscopic features (absorption and/or emission) upon reaction with the respective FG, such as the activatable "turn-on dye" Fluram or the chromogenic "chameleon dyes" IR797

(both for  $\text{NH}_2$  only); and (iii) cleavable reporters that allow for a determination of particle-bound labels, unbound reporters in the supernatant, and reporters cleaved off from the particle surface, such as the commercial crosslinker SPDP (*N*-Succinimidyl 3-(2-pyridyldithio)propionate, for  $\text{NH}_2$  groups) and its self-synthesized analogue *N*-APPA (*N*-(aminoethyl)-3-(pyridin-2-yl)disulfanyl)-propanamide, for COOH groups after activation with EDC/NHS or HATU). Labeling to carboxy groups was performed in all three approaches, a direct quantification of surface-bound dyes can be hampered by light scattering from the NP (for particles with diameters  $< 50$  nm) or by signal contributions from encoding dyes or the particle itself (in the case of absorptive and/or emissive NP such as metal particles and semiconductor quantum dots). Also, the signal intensity of surface-bound labels – especially for emission-based detection – can differ from that of the free reporters in solution, as photoluminescence is an environment-sensitive quantity and can be affected by quenching effects due to dye-dye or NP-dye interactions, which renders calibration tedious and erroneous. Thus, the conventional dyes NHS-fluorescein and 6-amino fluorescein (i) were only quantified via the unreacted (free) dyes in the supernatant, and the activatable dye Fluram and the chromogenic dye IR797 (ii) needed proper calibration with suitable FG-containing ligands having a similar chemical structure as the NP surface ligands, as a quantification in the supernatant is not possible here. In contrast, the cleavable reporters SPDP and *N*-APPA (iii) allow for the quantification of particle-bound reporters, unbound reporters in the supernatant, and reporters cleaved off from the particle surface, and thus, for a complete mass balance. Moreover, these labels can be also indirectly quantified via the formation thiol groups on the NP that could be measured with  $^{32}\text{S}$  ICP-OES and the Ellman's test (an optical assay for thiol groups).

#### Summary of results:

The conductometric titration and the three dye-labeling based optical assays for FG quantification were compared using commercial, amino- and carboxy-functionalized, 100 nm-sized polystyrene nanoparticles (PS NP) from Kisker Biotech GmbH (Germany), and the results are compared in **Figure 11 (top)**. The comparison reveals that conductometric titration yields a significantly higher FG concentration than the optical assays, as conductometric titration measures the total number of FG, whereas the dye-based optical assays detect the fraction of FG that are accessible for further (bio)functionalization. For amino groups, the FG concentration measured via conductometric titration could be verified with the Fluram assay after dissolution of the polymer matrix with THF, which allows all present FG groups to be accessible for labeling, and thus, also detects the total FG concentration. Comparison of the different dye labeling-based assays revealed a good agreement for all three approaches. The conventional fluorescein derivatives are spectrophotometrically and fluorometrically detectable, but can only be quantified indirectly via the amount of unreacted dyes in the (NP-free) supernatant to prevent signal distortions by light scattering and dye-quenching effects. This also applies for the activatable dye Fluram and the chameleon dye IR797, which is why Fluram could only be determined after NP dissolution with THF (the unreacted dye is unstable in aqueous solutions and cannot be detected at all), and IR797 was measured as unreacted dye in the supernatant and as labeled dye after NP dissolution with THF. However, both Fluram and IR797 requires calibration with model systems to account for target-specific changes in  $\epsilon(\lambda)$  and  $\Phi$ . The cleavable reporters SPDP and *N*-APPA, in contrast, allow for the spectrophotometric quantification of particle-bound reporters, unbound reporters in the supernatant, and reporters cleaved off from the particle surface, and thus, for a complete mass balance. Moreover, the cleavable reports enable the indirect FG quantification via the formation of thiol groups on the NP upon cleavage that can be measured with ICP-OES and the Ellman's assay (an already evaluated optical assay for thiol groups), and thus, for a straightforward and simple validation with other analytical methods relying on different detection schemes, as demonstrated in **Figure 11 (bottom)**.

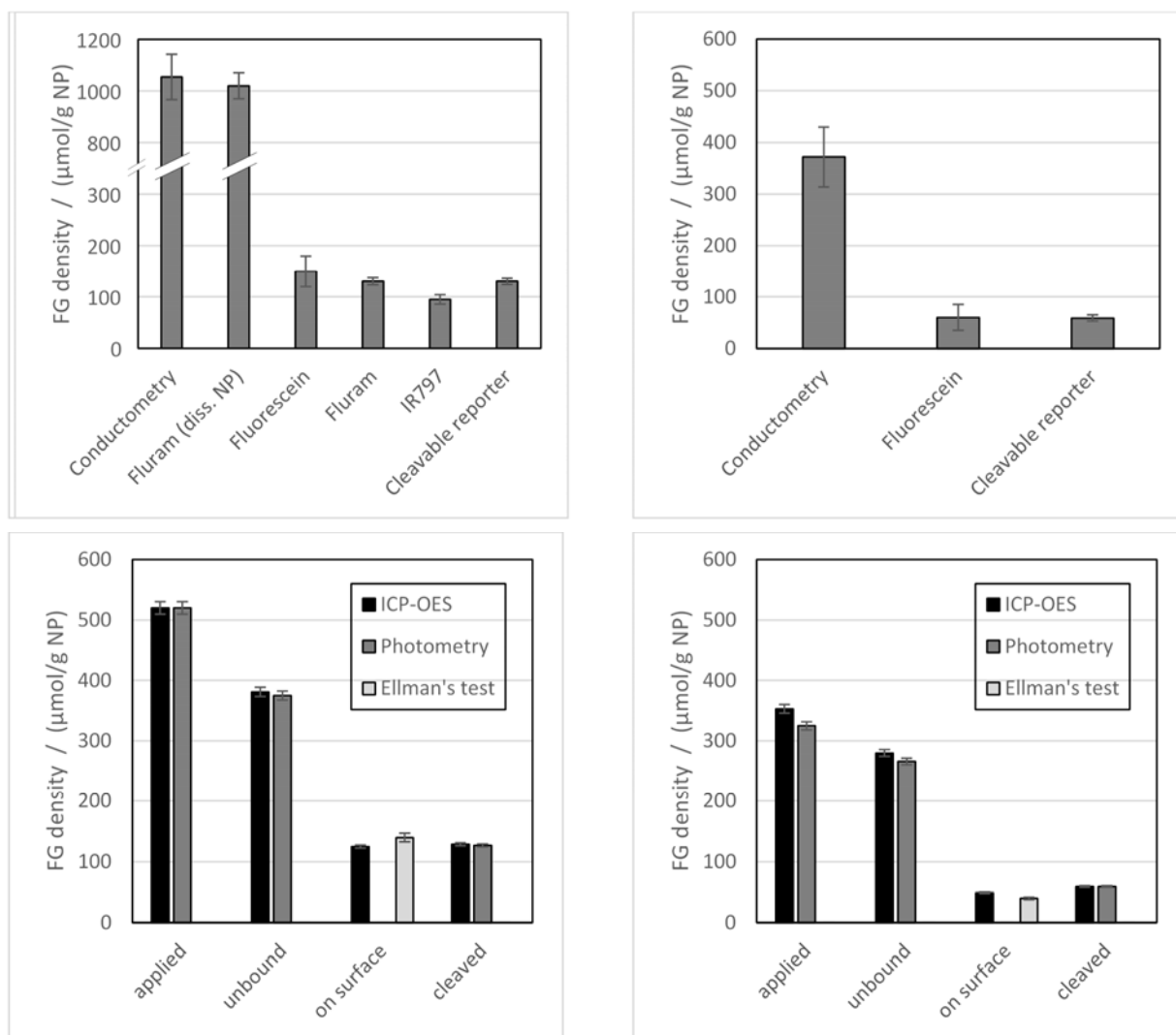


**Figure 11: Top:** Quantification of the total FG concentration and the concentration of accessible FG for commercial NH<sub>2</sub>-functionalized (*left*) and COOH-functionalized (*right*) 100 nm PS NP. Here, only ca. 12% of the NH<sub>2</sub> groups and ca. 16% of the COOH groups are accessible for further (bio)functionalization. **Bottom:** Validation of the FG quantification with the cleavable reporters SPDP for NH<sub>2</sub> groups (*left*) and *N*-APPA for COOH groups (*right*) using <sup>32</sup>S ICP-OES and the Ellman's test for the quantification of thiol groups that are formed on the NP upon reporter cleavage.

## Inter-laboratory studies

### *This Chapter addresses Objective 4*

A VAMAS-TWA2 (Surface Chemical Analysis) Project A19 Inter-laboratory study of the measurement of chemistry and thickness of nanoparticle coatings was completed. The key findings were that the following issues need to be addressed to ensure that comparable data is obtained by different laboratories: sample preparation protocols, instrument calibration and data interpretation. 21 participants from all regions of the world prepared and analyzed peptide-coated gold particle samples using either X-ray photoelectron spectroscopy (XPS) or low energy ion scattering (LEIS). The calculation method chosen by XPS participants contributed a variability of 67 % to the results. However, an acceptable variability of 12 % was achieved with a single calculation method, by choosing photoelectron peaks that were not adversely affected by instrumental transmission effects and the same reference data. The results from the LEIS participants were more consistent, with variability of less than 10 % in thickness and this is mostly due to a common method of data analysis. The importance of this activity is to demonstrate that the inter-laboratory *variability* of shell thickness measurements using surface analytical techniques is 10% and the individual laboratory *precision* can be better

than 5%. The Innanopart project has also shown that, using correct methods, the *accuracy* has similar magnitude to these other errors.

A **VAMAS-TWA34 (Nanoparticle populations) Project 10** interlaboratory comparison on the measurement of number concentration of nanoparticles was initiated. The study is underway and running in parallel with the **BIPM CCQM-P194 pilot study**, led by LGC, on the same materials. The materials chosen for the study are 30 nm gold nanoparticles and could become the first reference material with information on the nanoparticle number concentration available to stakeholders. This will enable the calibration of instruments and validation of methods with impact on a wide range of industrial sectors that make use of nanoparticles. The launch of this study had an overwhelming response, with 48 enrolled laboratories, for a total of 87 instruments across the globe over five measurement techniques: UV-Visible spectroscopy, particle tracking analysis (PTA), differential centrifugal sedimentation (DCS), single-particle inductively coupled mass spectrometry (sp-ICP-MS) and small angle X-ray scattering (SAXS). The samples were shipped to the participants in April and measurements will be performed. shortly.

## 5 Impact

The partners have presented the project results and progress in more than 40 different European and international conferences. 11 papers have been published, 1 has been submitted and several are in preparation. In addition, two book chapters on nanoparticle measurement have been published. All these activities, in addition to the contributions to standardisation bodies (see section below) aimed at promoting the uptake of methods and the validation of new reference materials. The project had a significant number of collaborators (nearly 20), many of whom participated in inter-laboratory studies. The project also retained an interested group of stakeholders to ensure the needs of interested parties were fed into the project.

A final Innanopart workshop was held at the Royal Society of Chemistry (RSC) headquarters, and attracted more than 120 international attendees from National Measurement Institutes, industry, academia, standardisation bodies, instrument manufacturers and regulators. The event created a forum for the discussion of critical requirements and state-of-the-art measurements for nanoparticle concentration. It highlighted the needs for further standardisation in the field, including the pressing requirement of nanoparticle reference materials with known number concentration to calibrate instruments, underpin reproducibility and develop new technologies such as nanoscale drug delivery vehicles in a safe and reliable manner.

### *Impact on industrial and other user communities*

The project had a growing number of collaborators to whom the project partners provided support and consultancy. As one of the industrial collaborators of this project, Malvern Panalytical approached NPL with their, now released, Zetasizer Ultra which combines multi-angle DLS (MADLS) and adaptive correlation. Malvern Panalytical had knowledge of the expertise within the consortium and wanted to validate the technique and benchmark it against other Malvern Panalytical products. NPL was able to provide both the materials and know-how to effect this successful comparison, which has resulted in a paper being drafted for submission.

The national measurement institute of Taiwan, ITRI, consulted NPL during the initiation of a large scale project to measure the size and concentration of particles in wastewaters. The analytical method to measure surface chemistry of nanoparticles, including sample preparation and core-shell structure characterisation, is available as measurement services at NPL and BAM.

A practical training course on DCS techniques for measuring particle number concentration has been completed, with excellent attendance from industries such as Syngenta, Astra Zeneca, BASF and Malvern and expert speakers from academia, industry and national laboratories, including the Australian NMI. A spICPMS data analysis workshop, which included hands-on training took place at RIKILT Wageningen in conjunction with the EU NanoDefine and NanoFASE projects which included industrial participants.

### *Impact on the metrology and scientific communities*

A VAMAS international inter-laboratory study on measuring shell thickness on particles using calibrated reference materials is complete and has been published. This work will enable valid, routine monitoring and quality control of surface chemistry for nanoparticle-based formulations and products.

An additional VAMAS international study on inter-laboratory particle number concentration has been initiated along with a parallel BIPM pilot study. Methods developed in this project have been disseminated through a

good practice guide, peer-reviewed papers, conferences, dedicated workshops and websites to ensure the widest possible benefit.

### *Impact on relevant standards*

The results of this project provided input to existing standards and stimulated the creation of new international standards which will enable both the concentration and surface chemistry of particles to be measured in a consistent and comparable manner. The partners have disseminated the results to a range of technical committees and standards bodies. Partners have contributed to a number of international standard committees: ISO TC229 (Nanotechnologies), ISO TC201 (Surface Chemical Analysis), ISO TC202 (Microbeam Analysis) and ISO TC24 SC4 (Particle Characterisation). In addition, this project provided input to

- IEC TS 62565-4-2:2018, Nanomanufacturing - Material specifications - Part 4-2: Luminescent nanomaterials - Detail specification for general lighting and display applications
- ISO 20579-4 "Surface Chemical Analysis - Sample handling, preparation and mounting - Part 4 – Reporting information related to the history, preparation, handling and mounting of nano-objects prior to surface analysis",
- ISO TS 19590 Nanotechnologies -- Size distribution and concentration of inorganic nanoparticles in aqueous media via single particle inductively coupled plasma mass spectrometry,
- ISO TS 21362 'Nanotechnologies -Application of field flow fractionation for characterization of nanomaterial contents',
- ISO TR 20489 'Separation and size fractionation for the characterization of metal-based nanoparticles in water samples',
- ISO 19668 Surface chemical analysis — X-ray photoelectron spectroscopy — Calculating and reporting detection limits for elements in homogeneous materials.
- ISO PWI 23484 Determination of particle concentration by small angle X-ray scattering (SAXS). Additionally a PWI on the measurement of core-shell nanoparticles using XPS has been initiated in ISO TC201.

### *Longer-term wider impact*

Typically more than half of the nanoparticles produced for high performance applications fail to meet specifications. Numerous cycles of production and measurement are required to optimise processes and counteract this failure rate. The current cost of validating nanomaterials by electron microscopy is approximately € 2000 per sample. The guidance, standards and cost effective methods developed in this project could reduce this cost by an order of magnitude. We envisage that such standards will strengthen and grow the current € 3 bn market in high performance nanoparticles.

This project extended nanometrology beyond the well-established measurement of size to enable routine monitoring of particle number concentration and chemistry. These measurements represent major progress in supporting the production of reliable nanomaterials. Through these advances in measurement, nanomaterial suppliers and users can have confidence that batch-to-batch variability will be minimised and, by providing international standards for these measurements, world-wide trade in nanomaterials and European competitiveness will be enhanced.

The emerging nanomaterials industry in Europe is at a critical juncture. The EU is rightly seen as the most cautious and conservative market for nanotechnological products because of imminent regulation and reporting requirements. It is imperative, therefore, that the EU is seen to be leading the global community in providing measurements and standards in support of its legislative ambitions. The European Commission has challenged nanomaterials manufacturers to state the composition of their materials. Those industries that meet the challenge will improve their productivity and competitiveness because of their greater understanding of their own products and their ability to provide specifications to their suppliers. This project offered a coordinated effort to establish the measurement framework to support EU companies in the production of better, more competitive products, develop methods and instrumentation to measure nanoparticles and to meet EU regulatory requirements.

The project has contributed to an improved acceptance of nanotechnology and nanotechnology-based products by society through the dissemination of validated protocols for measurement of nanoparticle number concentration and surface chemistry. This provides a reliable basis for the acceptance of nanoparticle-

containing products by the consumer. Moreover, by improving the measurement of nanoparticles produced for innovative applications, it has enabled industry to finely control the production of nanoparticles so that more reliable, efficient and new products can be generated with higher performance.

## 6 List of Publications

- A technique for calculation of shell thicknesses for core–shell–shell nanoparticles from XPS data. DJH Cant, YC Wang, DG Castner, AG Shard. *Surface and Interface Analysis* 48 (5), 274-282 (2016)
- Evaluation of Two Methods for Determining Shell Thicknesses of Core–Shell Nanoparticles by X-ray Photoelectron Spectroscopy. CJ Powell, WSM Werner, AG Shard, DG Castner. *The Journal of Physical Chemistry C* 120 (39), 22730-22738 (2016)
- Versailles project on advanced materials and standards interlaboratory study on measuring the thickness and chemistry of nanoparticle coatings using XPS and LEIS. NA Belsey, DJH Cant, C Minelli, JR Araujo, B Bock, P Brüner, et al. *The Journal of Physical Chemistry C* 120 (42), 24070-24079 (2016)
- Detection of suspended nanoparticles with near-ambient pressure x-ray photoelectron spectroscopy. M Kjaervik, A Hermanns, P Dietrich, A Thissen, S Bahr, B Ritter, E Kemnitz, W Unger. *Journal of Physics: Condensed Matter* 29, 474002 (2017)
- Shell thickness determination for PTFE-PS core-shell nanoparticles using scanning transmission X-ray microscopy (STXM). A Müller, S Swaraj, K Sparnacci, WES Unger. *Surface and Interface Analysis* (2018). DOI: 10.1002/sia.6464.
- Measuring the size and density of nanoparticles by centrifugal sedimentation and flotation. C Minelli, A Sikora, R Garcia-Diez, K Sparnacci, C Gollwitzer, M Krumrey, AG Shard. *Analytical Methods* 10 (15), 1725-1732 (2018)
- Measuring the Relative Concentration of Particle Populations using Differential Centrifugal Sedimentation. AG Shard, K Sparnacci, A Sikora, L Wright, D Bartczak, H Goenaga-Infante, C Minelli. *Analytical Methods* 10, 2647-2657 (2018)
- Evaluating the Internal Structure of Core–Shell Nanoparticles Using X-ray Photoelectron Intensities and Simulated Spectra. M. Chudzicki, W. S. M. Werner, A. G. Shard, Y.-C. Wang, D. G. Castner, and C. J. Powell. *J Phys Chem C*, dx.doi.org/10.1021/acs.jpcc.5b04517
- Chapter 4: Particle Number size distribution. H Goenaga-Infante, D Bartczak. *Nanomaterial characterization: an introduction*. DOI: 10.1002/9781118753460.ch4.
- Chapter 8: Surface Chemistry. N.A. Belsey, A.G. Shard, C. Minelli. *Nanomaterial characterization: an introduction*. DOI: 10.1002/9781118753460.
- Exposure of Mass-Selected Bimetallic Pt-Ti to Oxygen explored using the Scanning Transmission Electron Microscopy and Density Functional Theory. S Gholhaki, S-H Hung, CE Blackmore, AG Shard, Q Guo, K McKenna, RE. Palmer. *RSC Advances*. DOI: 10.1039/C8RA02449A.

## 7 Contact details

alex.shard@npl.co.uk